1 Supplementary Figures

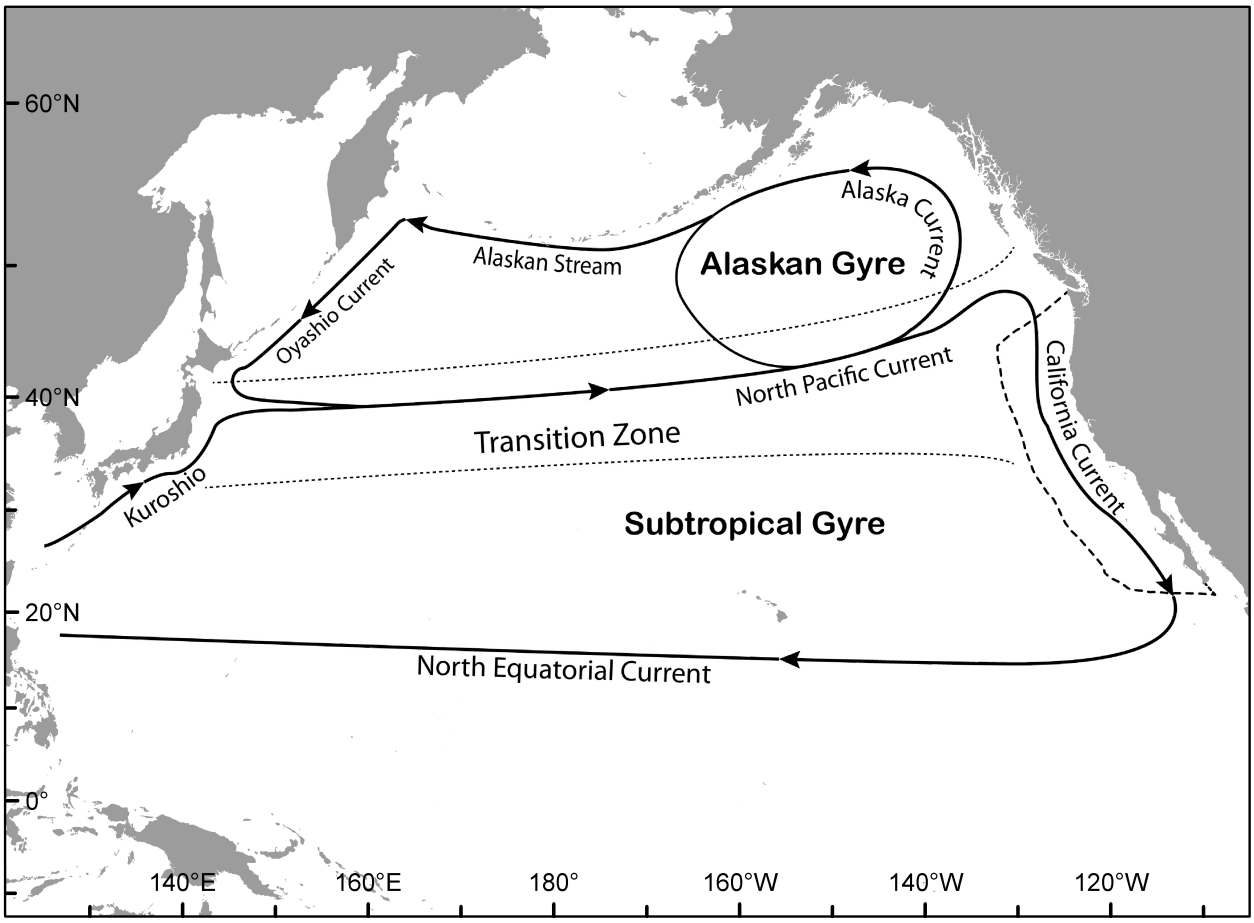

Supplementary Figure 1: Schematic of dominant ocean current features in the north Pacific Ocean. The California Current Large Marine Ecosystem is outlined (dashed line). The north Pacific Transition Zone is delineated by the dotted lines.

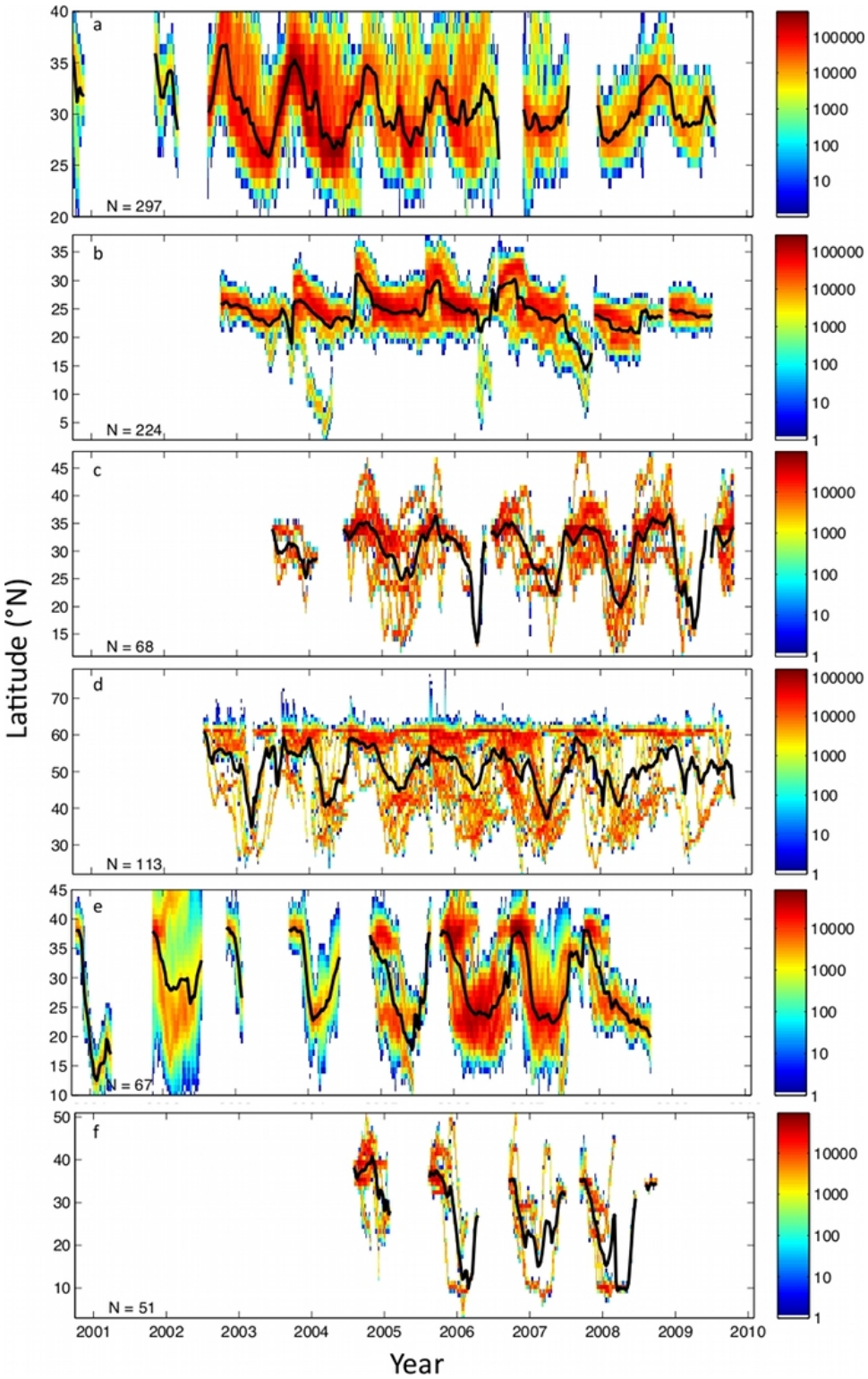

Supplementary Figure 2: Weekly mean latitude (black line) of predators that primarily inhabited or migrated to the CCLME. (a) Pacific bluefin tuna, (b) yellowfin tuna, (c) mako shark, (d) salmon shark, (e) white shark and (f) blue whale. Uncertainty in the estimated latitude was displayed by summing the posterior latitude samples within a 1 degree latitude band across the CCLME for each 1 week period from late 2000 to January 1, 2010. The color bar denotes the number of MCMC samples within the 1° latitude x 1 week cells. The number of tracks used for each species (N) is given in each panel.

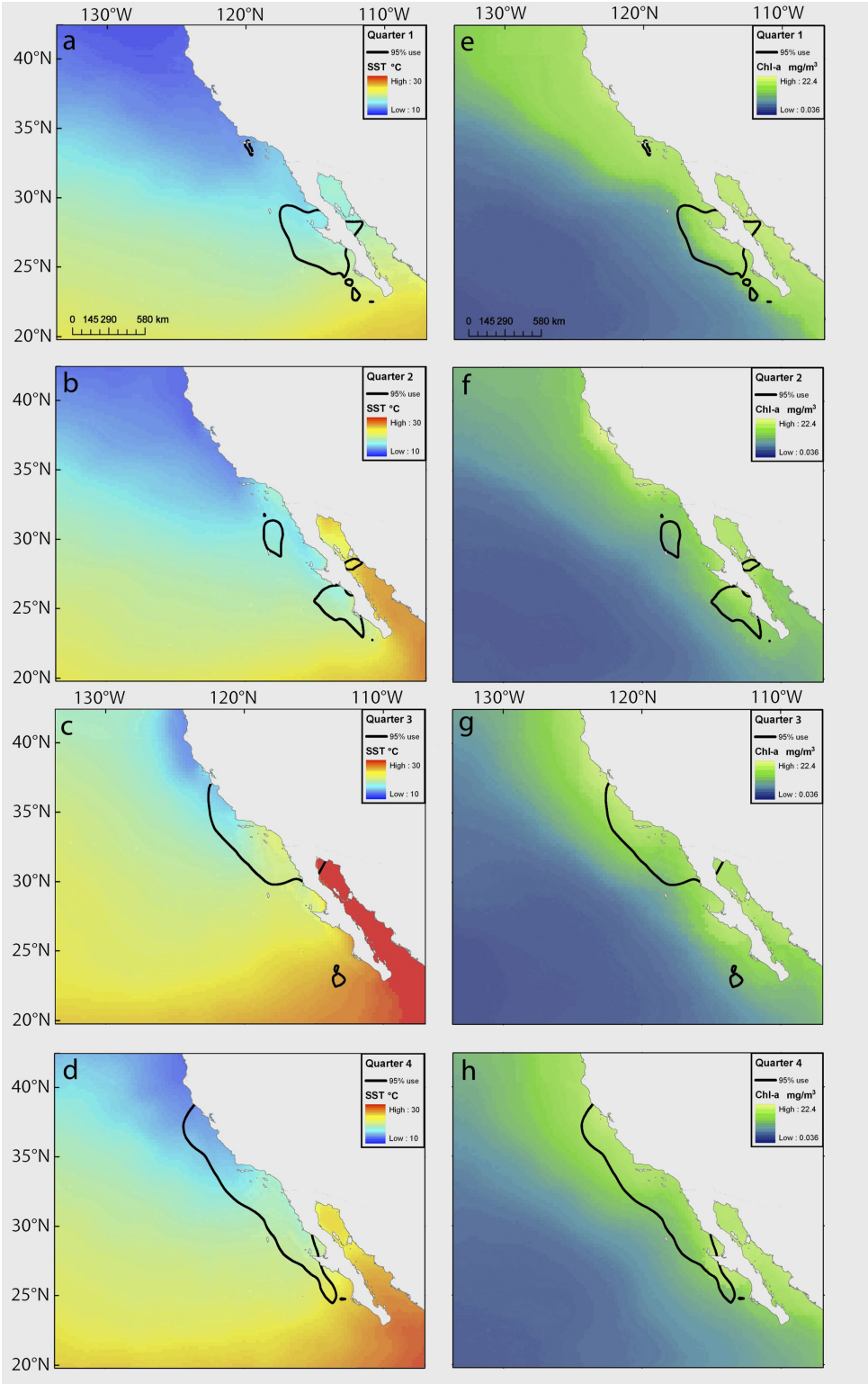

Supplementary Figure 3: Quarterly median sea surface temperatures (a-d) and chlorophyll-a from 2002-2009 (e-h). Contour lines represent the 95th percentile of relative density for the entire northeast Pacific Ocean shown in Figure 4a,b (the highest 5% of relative densities fall within the contour lines). The area of highest relative density moved northward as waters warmed and chlorophyll-a increased (quarter 3) and southward (quarter 4) as waters cooled.

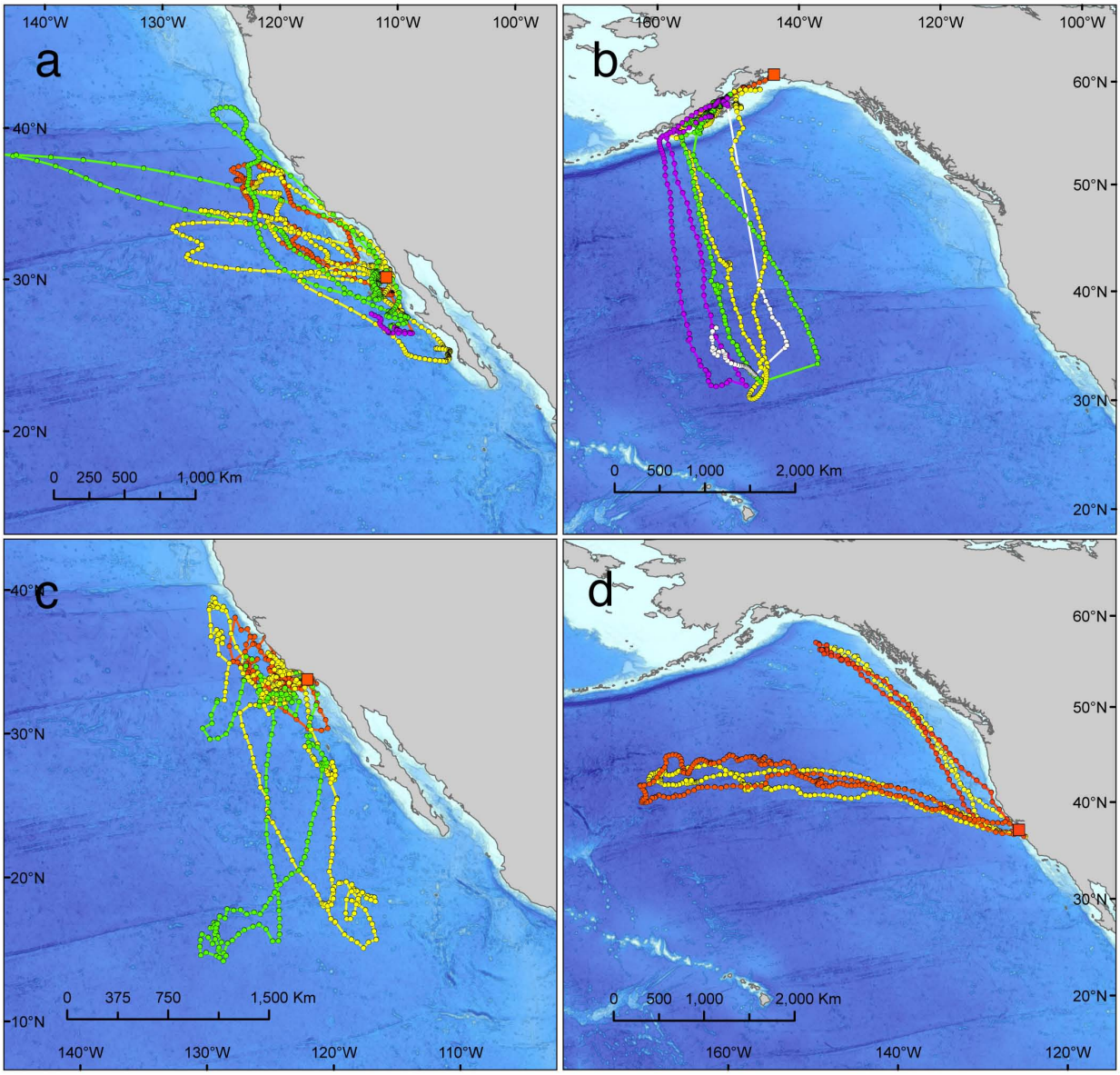

Supplementary Figure 4: Track duration and fidelity. Multi-year track displaying fidelity in consecutive years (a) Pacific bluefin tuna (903 days, year 1 ●, year 2 ●, year 3 ●, year 4 ●, year 5 ○), (b) Salmon shark (862 days) and (c) Mako shark (707 days). (d) Female northern elephant seals tagged in consecutive years show fidelity to rookery and migration paths. Lower track: female tracked during post-moult migrations of 2004 ● and 2005 ●. Upper track: female tracked during post-breeding migrations in 2005 ● and 2006 ●.

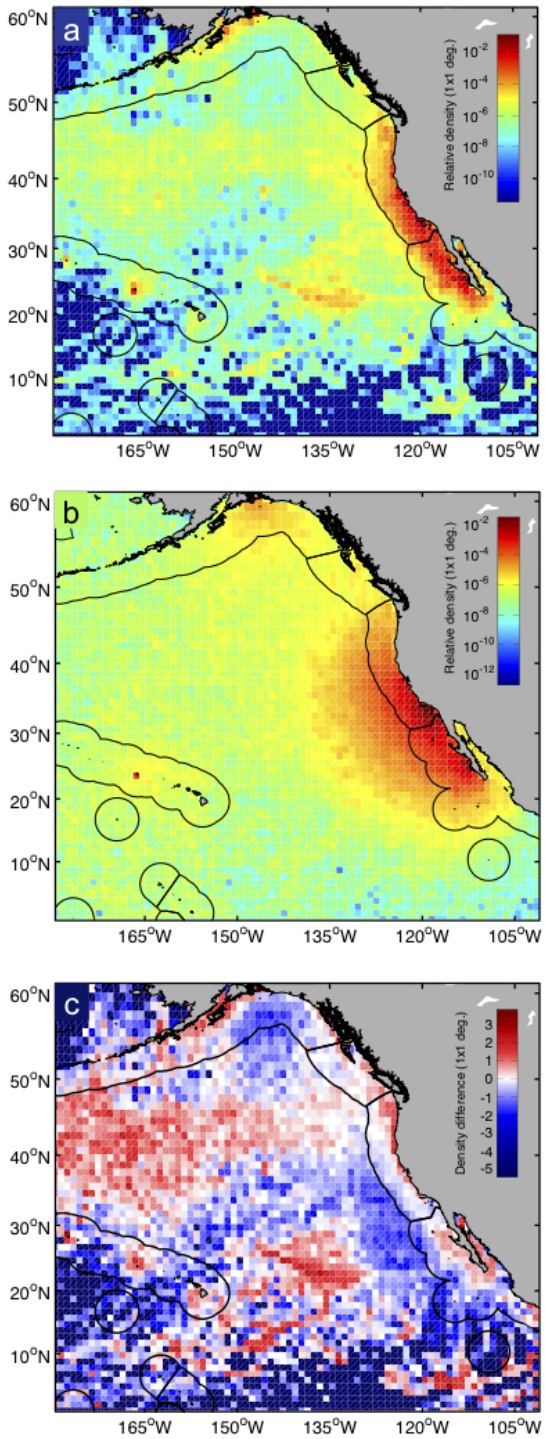

Supplementary Figure 5: Spatial densities of (a) tagged predators, (b) simulated predators and (c) their differences (observed - simulated). Observed and simulated densities were calculated after applying time-weighting for tag attrition and species normalizations; observed densities were calculated from posterior mean location estimates. The colour scale in panel c represents the difference in log spatial density.

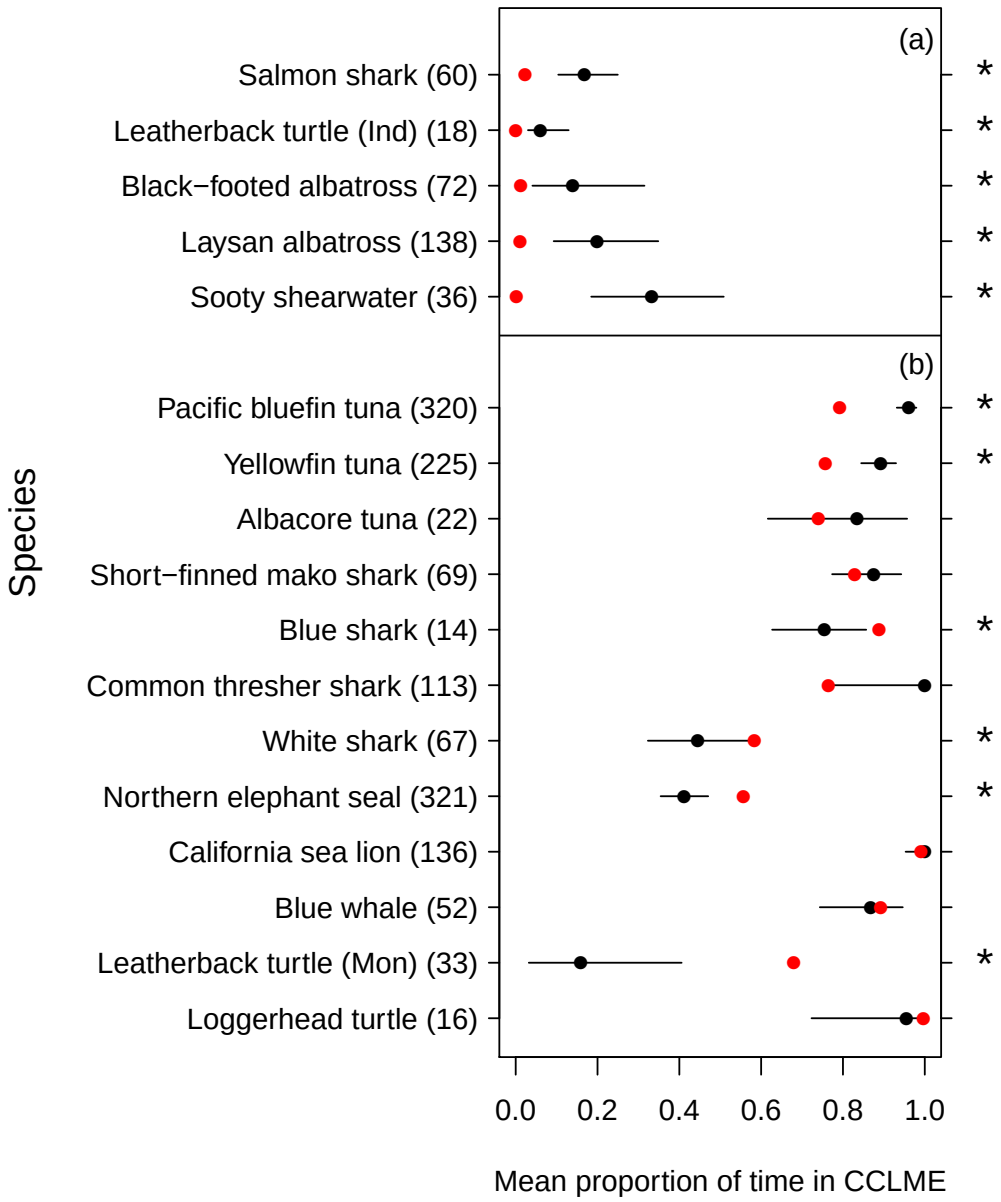

Supplementary Figure 6: Comparison of observed (black) with the simulated (red) mean proportion of time spent within the CCLME for each tagged species. Simulated mean proportions were obtained from the null model simulations of each species' movement patterns. The error bars around observed means are the binomial 95% confidence intervals. Significant differences between simulated and observed mean proportion of time spent in the CCLME are denoted with asterisks along the right vertical axis. (a) Species tagged outside the CCLME and (b) species tagged inside the CCLME. Sample sizes (number of track datasets) are in parentheses after each species name. Note that leatherback turtles were tagged at two distinct locations, in Monterey Bay, CA (Mon) and in Indonesia (Ind).

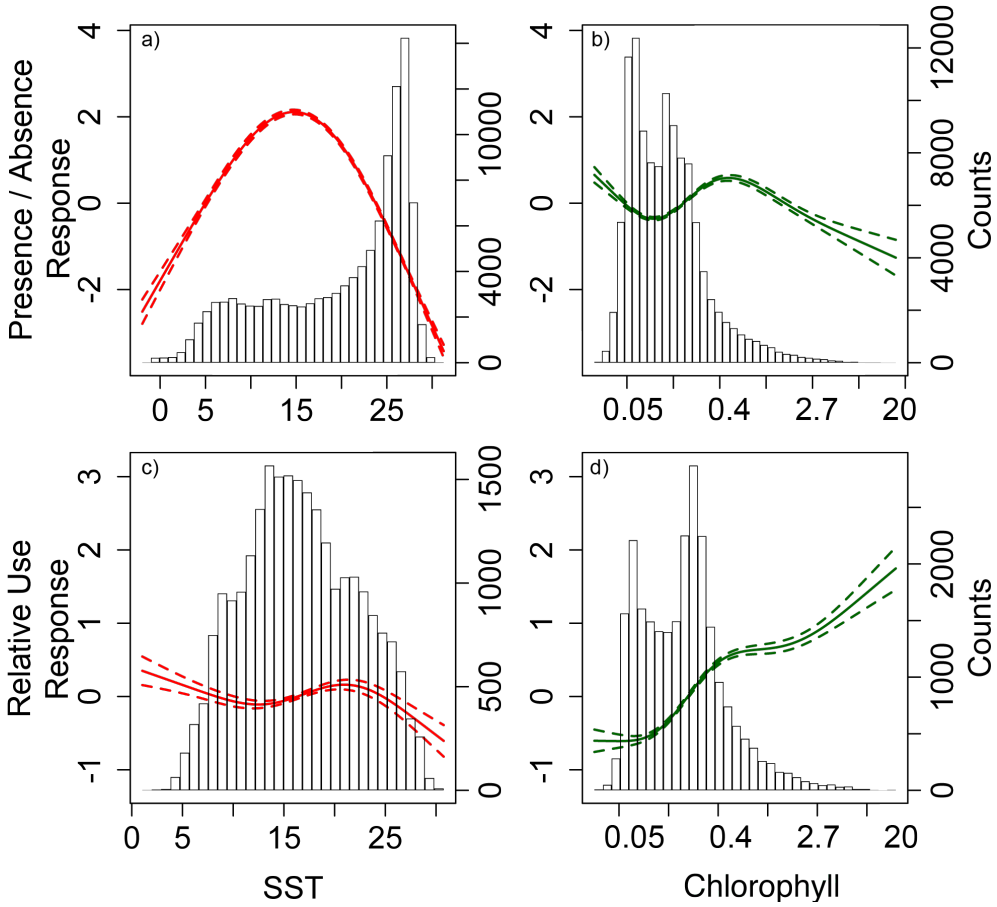

Supplementary Figure 7: Environmental correlates of large predator density.Generalized additive mixed model response curves from (a,b) binary presence / absence and (c,d) relative use models from the eastern Pacific. Model response is shown for (a,c) temperature (solid red lines) and (b,d) Chla(solid green lines), and dashed lines represent 95% confidence limits. Histograms show (a,b) the counts of total available habitat (i.e., number of 1-degree grid cells) in the eastern Pacific and (c,d) the counts of available habitat (i.e., number of 1-degree grid cells) in the eastern Pacific that was used by at least one TOPP species. The vertical axes are partial responses (estimated, centered smooth functions) on the scale of the linear predictor (logit in a,b; log in c,d).

2 Supplementary Methods

2.1 Electronic tracking data

TOPP scientists deployed a wide range of electronic tag models produced by a number of manufacturers including: Lotek Wireless (LTD 2310, 2400), Microwave Telemetry (Pico-100), Sirtrack (Kiwisat 202), Sea Mammal Research Unit (SLDR), Telonics (ST-6, ST-10 and ST-15) and Wildlife Computers (PAT Mk10, Avian Cricket, SPOT 4.0 and 5.0, Mk9 archival tags). In general tags were glued to pinnipeds[31], harnessed on to turtles[32], taped or banded to sea birds[33], implanted in tuna[34], bolted to dorsal fins[35] or sub-dermally attached to sharks[12] and sub-dermally attached to whales[36].

Test deployments to examine tag technologies and attachment strategies occurred on a subset of species from 1999-2001, and large-scale tag deployments commenced in 2002. Improvements in tag design, attachment, and database management led to the longest and largest dataset ever assembled on the movements of multiple species of marine vertebrates (Supplementary Tables 1 and 2).

Animal locations were observed by electronic tags using two primary methodologies: light-based geolocation and the Argos satellite network.

Archival tags and pop-up archival transmitting (PAT) tags, deployed on tuna, sharks and seabirds, used light-based geolocation. Light-based geolocations were estimated from day length and the time of local noon[37,38] and were further refined by matching satellite observed sea surface temperature (SST) to temperatures observed by the tag when possible[33,39]. This method does not require animals to surface and can be effectively performed using very small tags.

Satellite tags were deployed on marine mammals, large sea birds, sea turtles and sharks. Satellite tags perform best near the poles because of increased Argos satellite coverage and can collect as many as 40 locations per day at high latitudes, but will collect 3-10 locations a day near the equator under good conditions.

Supplementary Tables 2 and 3 provide detailed information on the tag deployments.

Supplementary Table 1: Summary of electronic tagging data by species, collected during TOPP from 2000-2009.

Common Name	N Tags[1]	Arch[2]	Sat Arch[3]	Argos Sat[4]	Datasets[5]	Days[6]	Mean Length (days)	Start Date	End Date	Max Length (days)
P. Bluefin Tuna	655	569	86		320	68123	212	08/05/02	07/27/09	946
Yellowfin Tuna	582	577	5		225	29060	129	10/13/02	07/09/09	1158
Albacore Tuna	296	296			22	4664	212	11/08/03	08/23/08	598
Swordfish*	29		29		0	167				
White Shark	97		97		67	12585	188	10/17/00	09/12/08	358
Salmon Shark	365	26	98	241	113	29873	264	07/15/02	09/22/09	1380
Mako Shark	213		65	148	69	15003	210	06/26/03	09/22/09	794
Blue Shark	198		54	144	60	5518	92	06/26/02	09/22/09	378
Thresher Shark	51		29	22	14	1952	139	05/05/04	12/23/08	245
Leatherback	182	32		150	96	26161	273	01/21/04	11/04/08	949
Loggerhead	17			17	16	2192	137	08/31/05	08/03/07	396
Sooty Shearwater	71	60		11	36	7667	213	01/28/05	11/02/06	332
Laysan Albatross	367	195		98	138	6196	45	12/15/02	01/12/09	268
Black-footed Albatross	169	93		49	72	4517	63	12/15/02	11/20/06	258
N. Elephant Seal	598	183	201	214	321	36753	114	06/22/02	09/22/09	273
C. Sea Lion	222	84	63	75	136	7630	56	04/08/03	08/19/09	282
N. Fur Seal*	10			10	9	891	99	10/04/06	05/09/07	217
Blue Whale	58		58		52	4689	90	07/29/04	09/28/08	288
Fin Whale*	2		2		2	318	159	08/02/04	07/29/07	306
Humpback Whale*	21		21		15	707	47	07/29/04	01/09/06	122
Sperm Whale*	19		19		8	72	9	04/20/08	05/16/08	19
Humboldt Squid*	44		44		0	330				
Ocean Sunfish*	40		36	4	0	318				
Total	4306	2115	1008	1183	1791	265386				

[1]Number of tags deployed [2]Number of archival tags deployed [3]Number of pop-up archival transmitting tags deployed [4]Number of Argos satellite tags deployed
[5]Number of viable datasets [6]Total number of tagging days

* These species were not used in analyses presented due to low numbers of viable datasets. Their tracks are present in Figure 1

Supplementary Table 2: Metadata for electronic tags deployed on study species. Sex codes are M = male, F = female and U = unknown. Information is presented only for species with viable datasets and that were used in subsequent analyses (see Table 1).

Common name	Scientific name	Years	Manufacturer	Tag models (n)	Total n	Sex (%)	Attachment methods
Pacific bluefin tuna	*Thunnus orientalis*	2002-2009	WC, Lotek	PAT2 (2), PAT3 (1), PAT4 (17), PAT-MK10 (25), Lotek 2310 (275)	320	100 U	[40,41]
Yellowfin tuna	*Thunnus albacares*	2002-2008	Lotek	Lotek 2310 (225)	225	100 U	[40,41]
Albacore tuna	*Thunnus alalunga*	2003-2006, 2008	Lotek	Lotek 2310 (22)	22	100 U	[40,41]
White shark	*Carcharodon carcharias*	2000-2008	WC	PAT2 (8), PAT3 (4), PAT4 (28), PAT-MK10 (27)	67	43 M, 34 F, 22 U	[42]
Salmon shark	*Lamna ditropis*	2002-2008	WC, SMRU	SPOT2 (17), SPOT3 (8), SPOT4 (21), SPOT5 (64), SPLASH (1), SRDL (2)	113	100 F	[13]
Shortfin mako shark	*Isurus oxyrinchus*	2003-2009	WC	SPOT2 (4), SPOT3 (2), SPOT4 (26), SPOT5 (36)	68	56 M, 43 F, 1 U	[13]
Blue shark	*Prionace glauca*	2004-2008	WC	SPOT2 (8), SPOT4 (32), SPOT5 (19)	59	39 M, 61 F	[13]
Common thresher shark	*Alopias vulpinus*	2004-2008	WC	SPOT4 (2), PAT4 (6) PAT-MK10 (6)	14	57 M, 43 F	[13]
Leatherback sea turtle	*Dermochelys coriacea*	2004-2008	SMRU, WC, Telonics	SRDL (73), SDRT16 (5), SPOT4 (5), MK10 (4), SPLASH (7), TELA2025 (4)	98	2 M, 24 F, 73 U	[5]
Loggerhead sea turtle	*Caretta caretta*	2005-2006	WC	SPLASH (9), SPOT4 (5), SPOT5 (2)	16	100 U	[24]
Sooty shearwater	*Puffinus griseus*	2005	Lotek, SirTrack	LTD2400 (25), SirTrack-PTT (11)	36	5 M, 7.5 F, 87.5 U	[6]

Supplementary Table 2: continued.

Common name	Scientific name	Years	Manufacturer	Tag models (n)	Total n	Sex (%)	Attachment methods
Laysan albatross	*Phoebastria immutabilis*	2002-2009	WC, MT, Lotek	SPOT4 (84), SPOT5 (45), Pico 100 (89), LTD2400 (29)	247	14 M, 15 F, 71 U	[33]
Black-footed albatross	*Phoebastria nigripes*	2002-2009	WC, MT, Lotek	Cricket (7), SPOT4 (74), Pico 100 (44), LTD2400 (24)	149	17 M, 16 F, 67 U	[33]
Northern elephant seal	*Mirounga angustirostris*	2002-2009	WC, SMRU, SirTrack, Telonics	SPOT4 (154), SPOT5 (7), SPLASH (2), SirTrack-PTT (4), Telonics-PTT (41), SRDL (70), MK10 (43)	321	21 M, 79 F	[31]
California sea lion	*Zalophus californianus*	2003-2008	WC, SirTrack, Telonics	SirTack-PTT (4), SRDL (37), SPOT4 (7), SPOT5 (43), MK10 (24), Telonics-PTT (21)	136	24 M, 76 F	[43]
Blue whale	*Balaenoptera musculus*	2004-2008	WC	WC-Custom (52)	52	100 U	[36]

Supplementary Table 3: Species tag deployment numbers and locations by year. Deployment numbers and locations are presented as single values for species with consistent deployment locations among years. Information is presented only for species with viable datasets and that were used in subsequent analyses (see Table 1).

Common name	Scientific name	Year(s) deployed	Number of datasets	Tagging location	Coordinates
Pacific bluefin tuna	*Thunnus orientalis*	2002	45	N Baja, MX	30.15°N, 116.91°W
		2003	80	N Baja, MX	29.26°N, 116.63°W
		2004	6	N Baja, MX	31.46°N, 117.51°W
		2005	78	N Baja, MX	31.79°N, 118.62°W
		2006	16	N Baja, MX	31.68°N, 116.91°W
		2007	14	N Baja, MX	31.68°N, 116.91°W
		2008	81	N Baja, MX	30.68°N, 117.43°W
Yellowfin tuna	*Thunnus albacares*	2002	13	N Baja, MX	25.74°N, 113.13°W
		2003	22	N Baja, MX	25.18°N, 114.44°W
		2004	40	N Baja, MX	30.99°N, 117.03°W
		2005	62	N Baja, MX	31.57°N, 118.31°W
		2006	53	N Baja, MX	23.63°N, 112.28°W
		2007	17	N Baja, MX	23.67°N, 111.92°W
		2008	18	N Baja, MX	31.09°N, 117.17°W
Albacore tuna	*Thunnus alalunga*	2003	7	S California, USA	29.27°N, 117.35°W
		2004	8	S California, USA	31.34°N, 117.66°W
		2005	5	S California, USA	31.80°N, 118.60°W
		2008	2	S California, USA	32.01°N, 119.18°W
White shark	*Carcharodon carcharias*	2000–03, 2006–07	39	Farallon Is, USA	37.69°N, 123°W
		2004	7	Point Reyes, USA	38.24°N, 123°W
		2005	21	Half Moon Bay, USA	37.4°N, 122.56°W
Salmon shark	*Lamna ditropis*	2002–08	113	Prince William Sound, USA	60.72°N, 146.12°W
Shortfin mako shark	*Isurus oxyrinchus*	2003-09	68	S California, USA	33.30°N, 118.48°W
Blue shark	*Prionace glauca*	2002–04	26	S California, USA	35.52°N, 121.32°W
		2005	1	S California, USA	33.17°N, 117.85°W
		2006	12	Baja, MX, USA	25.3°N, 113.52°W

Supplementary Table 3: continued.

Common name	Scientific name	Year(s) deployed	Number of datasets	Tagging location	Coordinates
		2007	11	Vancouver Is, CA	48.52°N, 126°W
		2008	9	S California, USA	33.67°N, 118.64°W
Common thresher shark	*Alopias vulpinus*	2004–08	14	S California, USA	33.78°N, 118.65°W
Leatherback sea turtle	*Dermochelys coriacea*	2004,2007	49	Costa Rica	10.33°N, 85.87°W
		2005	33	Indonesia	0.26°S, 132.67°E
		2004–05, 2007, 2009	16	Monterey Bay, USA	37.46°N, 122.38°W
Loggerhead sea turtle	*Caretta caretta*	2005–06	16	Baja, MX	25.76°N, 112.46°W
Sooty shearwater	*Puffinus griseus*	2005	21	Codfish Is, NZD	46.77°S, 167.65°E
		2005	4	Mana IS, NZD	41.10°S, 174.83°E
		2005	11	Monterey Bay, USA	36.83°N, 122.00°W
Laysan albatross	*Phoebastria immutabilis*	2003, 2005–06	96	Guadupe Is, MX	28.53°N, 118.18°W
		2002–09	151	Tern Is, USA	23.87°N, 166.28°W
Black-footed albatross	*Phoebastria nigripes*	2002–06	149	Tern Is, USA	23.87°N, 166.28°W
Northern elephant seal	*Mirounga angustirostris*	2002–09	281	Año Nuevo, USA	37.12°N, 122.34°W
		2005–06	40	San Benitos Is, MX	28.31°N, 115.59°W
California sea lion	*Zalophus californianus*	2005–07	18	Granitos Is, MX	29.54°N, 113.53°W
		2003–05	36	Monterey Bay, USA	36.83°N, 122.00°W
		2003–08	62	San Nicholas Is, USA	33.28°N, 119.57°W
		2005–06	20	San Miguel Is, USA	34.04°N, 120.44°W
Blue whale	*Balaenoptera musculus*	2004	9	Farallon Is, USA	37.42°N, 122.68°W
		2005	12	Monterey Bay, USA	36.83°N, 122.00°W
		2004–08	30	S California	34.15°N, 120.61°W
		2008	1	Costa Rica	8.77°N, 96.61°W

2.2 Gaps in tracking data

In most deployments, gaps in data did not exceed the state-space model (SSM) location estimate frequency of 1 estimate per day. Gap frequency varied by species and tagging method (Supplementary Table 4). Where gaps were long ($>$ 20 days) tracks were split into segments and reassembled after SSM filtering (see "State-space models", below) without including estimated locations during the gaps. This prevented us from introducing unrepresentative estimated locations that were not sufficiently constrained by data into any of the figures or subsequent analyses using the SSM-filtered locations.

Supplementary Table 4: Median and (mean) number of gaps of a given length per track by species. In most taxa, more than half of tracks contained no gaps greater than 5 days (medians = 0 in the 5 d column). Only in leatherback sea turtles and salmon sharks did more than half the tracks contain gaps greater than 10 days. Gaps up to 20 days are robustly handled by SSM fitting[44]. Tracks with gaps longer than 20 days were split into separate segments at the gap and the period of the $>$ 20 d gap was discarded from the analysis.

Species	Frequency of gaps					Tag type	N tracks
	2 d	3 d	5 d	10 d	20 d		
Bluefin Tuna	3 (7.11)	1 (2.15)	0 (0.63)	0 (0.1)	0 (0.03)	geoloc*	320
Yellowfin Tuna	1 (2.87)	0 (0.74)	0 (0.19)	0 (0.04)	0 (0.01)	geoloc	225
Albacore Tuna	14 (16.1)	8 (7.74)	3 (3.18)	0 (0.5)	0 (0.09)	geoloc	22
White Shark	2 (2.51)	2 (2.31)	2 (1.61)	0 (0.57)	0 (0)	geoloc	67
Salmon Shark	21 (28.09)	12 (18.43)	6 (9.5)	2 (3.3)	0 (0.85)	Argos	113
Shortfin mako Shark	21.5 (22.4)	8 (9.51)	2 (3.26)	0 (0.71)	0 (0.1)	Argos	68
Blue Shark	16 (20.72)	8 (11.47)	4 (4.53)	0 (0.94)	0 (0.09)	Argos	59
Common thresher Shark	2 (1.57)	0 (0.43)	0 (0.43)	0 (0.14)	0 (0)	geoloc	14
Sooty Shearwater	0 (2.36)	0 (1)	0 (0.4)	0 (0.08)	0 (0)	geoloc	36
Laysan Albatross	0 (0.39)	0 (0.29)	0 (0.2)	0 (0.06)	0 (0.02)	geoloc	247
Blackfooted Albatross	0 (0.47)	0 (0.33)	0 (0.22)	0 (0.14)	0 (0.06)	geoloc	149
Leatherback Turtle	15 (25.06)	5 (9.44)	2 (4.44)	1 (1.51)	0 (0.66)	Argos	98
Loggerhead Turtle	0 (0.79)	0 (0.79)	0 (0.64)	0 (0.29)	0 (0.29)	Argos	16
N. Elephant Seal	0 (4.16)	0 (2.46)	0 (1.01)	0 (0.4)	0 (0.2)	Argos	321
California Sea Lion	0 (0.51)	0 (0.3)	0 (0.22)	0 (0.19)	0 (0.13)	Argos	136
Blue Whale	3 (7.14)	2 (3.82)	0 (1.19)	0 (0.26)	0 (0.05)	Argos	52

* geolocation

2.3 State-space models

State-space models (SSMs)[14] were fitted to all the tracking data to account for observation error, to regularize animal location estimates in time and to interpolate over small gaps resulting from missing observations of animals locations. We collectively refer to these objectives as "filtering" and used a Bayesian implementation to filter both the Argos- and geolocation-based tracking data. The process model assumes that the first

differences, $\mathbf{d}_t$, in an animal's locations are a correlated random walk with mean turning angle θ and move autocorrelation γ:

$$\mathbf{d}_t = \gamma \mathbf{T}(\theta)\mathbf{d}_{t-1} + \boldsymbol{\eta}_t \tag{1}$$

where $\mathbf{d}_t$ is the first difference in the true but unobserved locations $\mathbf{x}_t$ and $\mathbf{x}_{t-1}$ and $\mathbf{T}(\theta)$ is a matrix describing the rotation between $\mathbf{d}_t$ and $\mathbf{d}_{t-1}$,

$$\mathbf{T}(\theta) = \begin{pmatrix} \cos\theta & -\sin\theta \\ \sin\theta & \cos\theta \end{pmatrix} \tag{2}$$

and $\boldsymbol{\eta}_t$ is the stochastic deviation in movement between times t and $t-1$, which is assumed to be normally distributed with mean 0 and variance-covariance matrix $\boldsymbol{\Sigma}$:

$$\boldsymbol{\Sigma} = \begin{pmatrix} \sigma^2_{\text{lon}} & \rho\sigma_{\text{lon}}\sigma_{\text{lat}} \\ \rho\sigma_{\text{lon}}\sigma_{\text{lat}} & \sigma^2_{\text{lat}} \end{pmatrix} \tag{3}$$

The process model in (Eq. 1) was fitted to tracking data using an observation model that allowed irregularly timed observations with time-varying non-normal errors[14]:

$$\mathbf{y}_i = \boldsymbol{\mu}_i + \boldsymbol{\epsilon}_i \tag{4}$$

where $\mathbf{y}_i$ is the ith $(i = 1, 2, \ldots, n)$ pair of longitude and latitude data, $\boldsymbol{\mu}_i$ is the corresponding true longitude and latitude and $\boldsymbol{\epsilon}_i$ are random, serially independent observation errors. The estimated true locations, $\boldsymbol{\mu}_i$, were calculated from the estimated states that were regular in time, $\mathbf{x}_t$, according to:

$$\boldsymbol{\mu}_i = (1 - j_i)\,\mathbf{x}_{t-1} + j_i\mathbf{x}_t \qquad \text{for} \qquad i \in I_t \tag{5}$$

where I_t is the set of observations that occurs between times $t-1$ and t and the scalar $j_i (0 < j_i < 1)$ is the proportion of this time step that elapsed prior to $\boldsymbol{\mu}_i$. This approach results in a linear interpolation of the $\boldsymbol{\mu}_i$'s along the straight line paths between the regularly estimated states, $\mathbf{x}_{t-1}$ and $\mathbf{x}_t$.

Errors in Argos data were assumed to be scaled *t*-distributed[19] so that $\epsilon_{i,\text{lon}} \sim t\left(0, \psi\tau_{\text{lon},q_i}, \nu_{\text{lon},q_i}\right)$ and similarly for latitude, where q_i is the Argos location quality class of $\mathbf{y}_i$, $\tau_{\text{lon},q}$ and $\tau_{\text{lat},q}$ and $\nu_{\text{lon},q}$ and $\nu_{\text{lat},q}$, are the precision scale parameters and degrees of freedom of the *t*-distribution, respectively, for location quality class *q*, and ψ is an estimated parameter that allows for variability in the scale of errors arising from variability among tags. We fixed the values of $\tau_{\text{lon},q}$, $\tau_{\text{lat},q}$, $\nu_{\text{lon},q}$ and $\nu_{\text{lat},q}$ for each of the 6 Argos location quality classes (3, 2, 1, 0, A, B) at values derived from an analysis of Argos data from seals in captivity at a known location (Supplementary Table 5)[45,14]. Location quality class Z was assumed to be of the same quality as class B.

Errors in geolocation data were assumed to be normally distributed so that $\epsilon_{i,\mathrm{lon}} \sim N(0, \tau_{\mathrm{lon}})$, and similarly for latitude. The precisions of geolocation errors, τ_{lon} and τ_{lat}, were estimated from double-tagging experiments and captive studies (see next section).

Estimated locations were effectively fixed for known deployment and recovery locations by assuming very high data precision. For models fitted to Argos data, deployment and recovery location data were assumed to be t-distributed with an error *SD* of 10 m and 100,000 degrees of freedom. For models fitted to geolocation data, deployment and recovery location data were assumed to be normally distributed with the same error *SD*.

The state-space model was fitted separately to each track using the software WinBUGS that conducts Bayesian statistical analyses using Markov chain Monte Carlo (MCMC) sampling[46]. For each track, 2 MCMC chains each of length 10,000 were run and a sample of 2,000 from the joint posterior probability distribution was obtained by discarding the first 5,000 iterations and retaining every 5th of the remaining iterations. Supplementary Fig. 8 shows the fit of the state-space model to six example Argos and geolocation tracks.

We assessed the quality of the SSM fit for each individual track. The SSM fits to Argos and geolocation observations were visually inspected for obvious problems like poor fits to the data and unrealistic estimated movements. MCMC algorithm convergence was assessed using the $\hat{R}$ statistic. $\hat{R}$ is the ratio of variances for the parameters and states between the MCMC chains, and when models are well converged, values should be near 1[47]. In almost all cases $\hat{R}$ values were very near 1. When they were not, usually only a single estimated location was involved produced by a single bad observation. Eliminating at most a few problematic data (or assigning these data a lower location quality class) usually solved the problem. Location estimates that were made from periods when there were large data gaps ($>$ 20 days) were dropped from the analysis, as model fits are not well constrained when data are completely absent. Tracks with a poor fit due to uncorrectable or intractable problems were discarded (e.g., early failure or malfunctioning of tags).

Supplementary Table 5: Fixed error distributions for Argos data of different location quality classes used in the filtering model. Errors were assumed to be *t*-distributed with a scale parameter expressed here as *SD* (degrees of longitude or latitude) and ν degrees of freedom. These values are from an analysis[14] of Argos data from seals in captivity at a known location[45].

Location quality class	SD_{lon}	ν_{lon}	SD_{lat}	ν_{lat}
3	0.0026	3.1	0.0011	2.1
2	0.0028	2.0	0.0023	6.3
1	0.0081	2.3	0.0041	3.9
0	0.019	2.0	0.014	2.0
A	0.0046	2.0	0.0046	2.0
B	0.038	2.0	0.027	2.0

2.4 Estimating geolocation errors

A challenge to analyzing our dataset was the mixture of technologies that were used to collect location data from the multiple animals observed. Argos location and geolocation estimates have substantially different

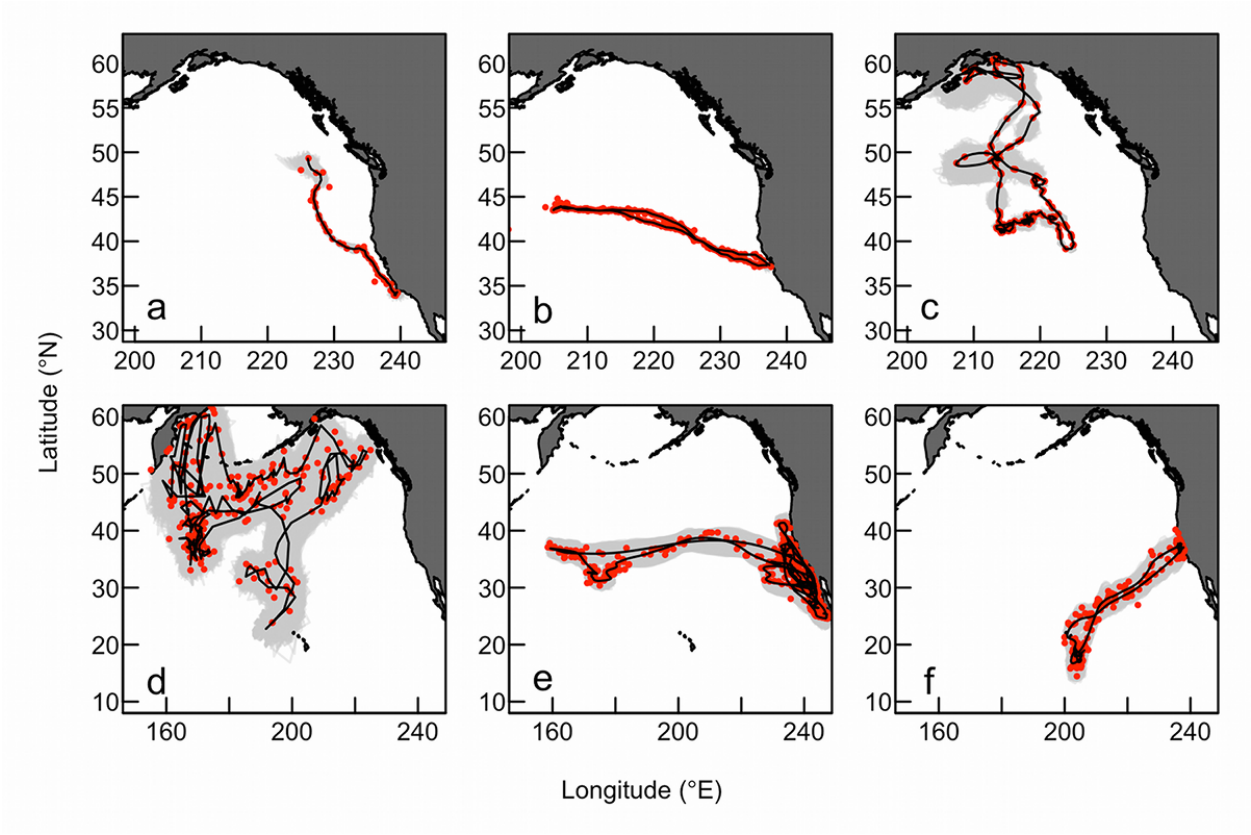

Supplementary Figure 8: State-space model fitted to three example Argos tracks (a - blue whale, b - northern elephant seal, c - salmon shark) and 3 example geolocation tracks (d - Laysan albatross, e - Pacific bluefin tuna, f - white shark). Red points represent Argos location and geolocation estimates and solid black lines represent the mean estimated paths from the fitted state-space model. The light grey areas represent the full posterior probability distribution of the estimated paths as approximated by a sample of 2000 paths from the posterior obtained using MCMC sampling.

error precisions associated with them, the former generally being higher. State-space methods have been developed for filtering geolocation data and estimating their error precisions[48,49], however, the underlying process model and statistical framework in those studies differed from our filtering model. In order to produce consistent, comparable filtered tracks across technologies, we chose to use the same filtering model for Argos and geolocation data. It is difficult to estimate the error and bias in geolocation data given only those data, particularly for short tracks. In a state-space framework, the estimation of the errors and bias can be confounded with the estimation of the parameters of the movement model. Furthermore, large systematic biases in geolocation data can only be determined by having more accurate data on a tag's location. Because of these difficulties in estimating geolocation errors from geolocation data alone, we derived independent estimates of the precision of geolocation data from separate studies in which tags were deployed on captive animals at known locations or 'double-tagging' experiments in which wild animals carried both geolocation tags and Argos tags (Winship *et al.*, in review). We fixed the error precisions of the geolocation data for a given technology at the estimates from these analyses of data from the same technology (Supplementary Table 6). The precision of geolocation errors can vary among individual tracks even within a single technology. Because we fixed the precision of geolocation errors at a single value for each technology, some individual tracks will have been undersmoothed and some will have been oversmoothed. Nevertheless, in the absence of other data for the geolocation tracks, the fixed estimates that we assumed were the best information available.

The precision of archival tag geolocations for tuna was estimated from archival tag data on 37 captive Pacific bluefin tuna at two known locations. Double-tagging data were available from blue (n=15), Galápagos (n=3), mako (n=25), and salmon sharks (n=23). Only salmon shark data south of $50°$N were considered for these analyses, as geolocation errors north of this latitude are greater and are not representative of the errors at the latitudes used by white sharks. Errors in PAT tag geolocations of white sharks were estimated from the PAT/Argos double-tagging experiments on the four other shark species whose locations overlapped latitudinally. Errors in archival tag geolocations of birds were estimated from archival/Argos double-tagging experiments on two albatross species, black-footed (n=12) and Laysan albatrosses (n=15).

Two datasets, Argos location and geolocation, were available for each double-tagged animal. The state-space filtering model was fitted simultaneously to both datasets for each individual to estimate the geolocation error precision. Supplementary Fig. 9 illustrates the model fit for an example track. We only analyzed data from individuals with $\geq$5 geolocations and we only analyzed geolocation data from dates with corresponding Argos data. We assumed wide, flat prior probability distributions for the model parameters. Samples from the joint posterior probability distribution were obtained by running two chains each of length 120,000, of which the initial 20,000 samples were discarded, and every 100^{th} of the remaining samples were retained for a total sample size of 2,000. Convergence of the error parameter estimates was assessed by examining the potential scale reduction factor ($\hat{\text{R}}$).

We calculated mean estimates of geolocation errors in longitude and latitude for each individual animal, species and species group (sharks, black-footed albatross and Laysan albatross). We report the estimated geolocation errors as *SD*s where $SD_{\text{lon}} = \sqrt{\frac{1}{\tau_{\text{lon}}}}$, and similarly for latitude. For each individual i, the samples of SD_{lon} and SD_{lat} from the joint posterior probability distribution were log-transformed and means and variances were calculated ($\log SD_{\text{lon},i}$ and $\sigma^2_{\log SD_{\text{lon},i}}$, respectively, and similarly for latitude). Each group mean was then calculated on the log-scale ($\log \overline{SD}_{\text{lon}}$) as the average of the individual means weighted by the inverse of their variance[50]:

$$\log \overline{SD}_{\text{lon}} = \frac{\sum_i W_i \log SD_{\text{lon},i}}{\sum_i W_i} \tag{6}$$

where

$$W_i = \frac{1}{\sigma^2_{\log SD_{\mathrm{lon},i}}} \tag{7}$$

The variance of the group mean on the log-scale ($\sigma^2_{\log \overline{SD}_{\mathrm{lon}}}$) was calculated as[64]:

$$\sigma^2_{\log \overline{SD}_{\mathrm{lon}}} = (\sum_i W_i)^{-1} \tag{8}$$

The group means and their variances were then back-transformed according to:

$$\overline{SD}_{\mathrm{lon}} = e^{\log \overline{SD}_{\mathrm{lon}}} \tag{9}$$

and

$$\sigma^2_{\overline{SD}_{\mathrm{lon}}} = e^{2 \log \overline{SD}_{\mathrm{lon}}} e^{\sigma^2_{\log \overline{SD}_{\mathrm{lon}}}} (e^{\sigma^2_{\log \overline{SD}_{\mathrm{lon}}}} - 1) \tag{10}$$

The *SD*s of tuna geolocation errors were calculated from the root mean square error (RMSE) between geolocation estimates and known locations of individual captive Pacific bluefin tuna in open sea pens (3538 and 2462 longitude and latitude geolocations, respectively). The overall pooled RMSE was calculated from the individual RMSEs according to the standard equation for a pooled variance estimate. A double-tagging experiment on 9 free-ranging California sea lions in a different geographic area resulted in similar precision estimates for this type of archival tag (Winship *et al.*, in review).

Supplementary Table 6: Fixed error *SD*s (degrees) of geolocation data used in the filtering model. The *SD*s of geolocation error estimates from the analysis of double-tagging data are also presented.

Species	$\overline{SD}_{\mathrm{lon}}$	$\sigma_{\overline{SD}_{\mathrm{lon}}}$	$\overline{SD}_{\mathrm{lat}}$	$\sigma_{\overline{SD}_{\mathrm{lat}}}$	Species estimated from
white shark	0.64	0.012	1.9	0.035	4 shark spp.
black-footed albatross	3.8	0.27	1.9	0.13	black-footed albatross
Laysan albatross, sooty shearwater	1.9	0.090	1.2	0.056	Laysan albatross
P. bluefin, yellowfin, albacore tuna	0.77		1.9		Pacific bluefin tuna

2.5 Behavioural switching analyses

A switching state-space model (SSSM) was used to discriminate between latent resident (slow, area restricted movements) and transient (fast, directed movements) behavioral states in a subset of species' tracks. Stochastic switching models have been used to infer hidden patterns from data in fields such as Ecology[51,52,53], Epidemiology[54] and Econometrics[55,56]. We use the state-space model described in Eqns 1-5 and allow stochastic switching between two sets of the movement parameters, γ and θ, one for each assumed behavioral state. The switching is governed by a simple discrete Markov chain process commonly used in behavioural ecology[57]. The SSSM has two process models, one for each assumed behavioral state:

$$\mathbf{d}_{t,k} = \gamma_{b_{t,k}} \mathbf{T}(\theta_{b_{t,k}}) \mathbf{d}_{t-1,k} + \boldsymbol{\eta}_t \tag{11}$$

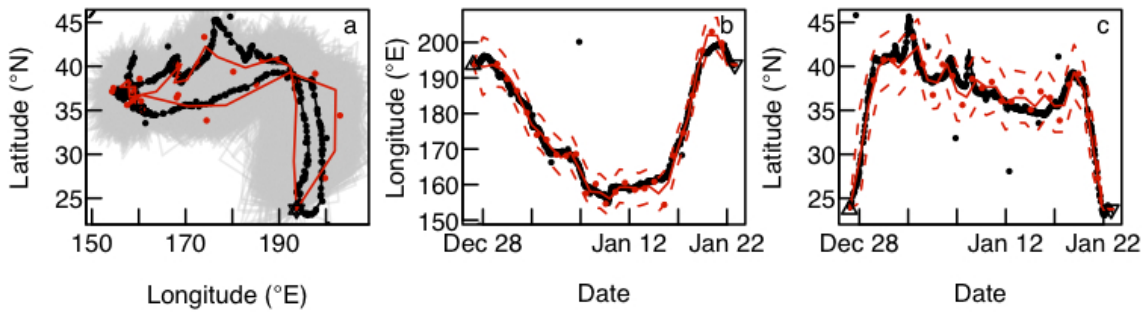

Supplementary Figure 9: State-space model fitted to Argos and geolocation data for an example Laysan albatross track. Black and red points represent Argos and geolocation data, respectively. Solid black lines represent the mean estimated path from the state-space model fitted to Argos and geolocation data simultaneously. For comparison, the solid red lines represent the mean estimated path from the state-space model fitted to only the geolocation data with the error *SD*s fixed at their mean estimates (2.4° and 1.4° for longitude and latitude, respectively). Triangles indicate known deployment and inverted triangles indicate known recapture locations. The light grey lines in panel a represent the full posterior probability distribution of the estimated path from the model fitted to only geolocation data as approximated by a sample of 2000 paths from the posterior obtained using MCMC sampling. In panels b and c, dashed lines represent intervals of 95% posterior probability for estimated locations from the two models.

where $b_{t,k}$ is the behavioral state at time t for individual k, $b_{t,k} = 1$ (transient) or 2 (resident). Switches between behavioral states are modelled by assuming that an individual can decide to change from the current state to another one with a fixed probability given by the Markov chain [14]:

$$Pr(b_{t,k} = i | b_{t-1,k} = j) = \alpha_{ij} \tag{12}$$

where α_{ij} is the probability of the animal being in behavioral state i at time t given that it was in behavioral state j at time $t-1$. We estimate α_{11}, the probability of remaining in the transient state, and α_{12}, the probability of switching from the resident to the transient state. The probabilities of the two other possible transitions are the complements.

The process model in Eqn. 11 was linked to the observation model described in Eqns 4-5.

The switching model was fitted as a hierarchical model to all tracks simultaneously within a species, allowing improved estimation of the behavioural state indices, $b_{t,k}$, for all individuals. Information about the movement parameters γ and θ was shared across all tracks by assuming the value of these parameters for a given behavioral state were the same for all individuals[58]. This is the simplest approach given that we are only interested in the $b_{t,k}$'s, and not γ or θ, for each individual.

Tracks were selected from each of 9 species; white shark (n=10), mako shark (n=10), salmon shark (n=10), Pacific bluefin tuna (n=10), yellowfin tuna (n=10), blue whale (n=10), blue shark (n=10), northern elephant seal (n=10 female, 10 male), and leatherback turtle (n=10). Each species spent prolonged periods within the California Current, or had a tendency to travel to and from the California Current. These tracks were

selected to represent the "average" or predominant movement pattern(s) exhibited by each species.

The switching state-space model was fitted to all datasets with a 1-day time-step.

2.6 Weighting and normalization

Multi-species electronic tagging datasets have biases associated with varying track durations (among individuals within a species) and sample sizes (among deployments, life history stages, and years within a species and among years across species). For all species, the number of tagged individuals decreased with time since deployment due to loss of battery power, biofouling, premature detachment, or mortality. Consequently, we applied a weighting scheme to the location estimate dataset to account for a high abundance of abbreviated tracks near the tagging location. Secondarily, we normalized the dataset by species to account for over-representativeness of species with large sample sizes.

2.6.1 Weighting to account for unnaturally abbreviated tracks

Estimating space-use from electronic tagging data can be problematic due to the abrupt end of records associated with tag failure, early release, and commercial harvest. In our dataset, these mechanisms resulted in a high number of short duration tuna, shark, whale and turtle tracks, biasing spatial coverage of the dataset toward the tagging locations, and obscuring ecological patterns. We accounted for skewed spatial coverage due to an overabundance of short tracks by applying a weighting scheme to each location.

First we developed a basic time weighting scheme, whereby for a given species, we weighted each location estimate by the inverse of the number of individuals of that species that had location estimates for the same relative day of their track:

$$w_{it} = 1/n_{jt} \qquad \text{for} \qquad i \in I_j \tag{13}$$

where w_{it} is the weight for the tth location estimate of the ith individual's track, n_{jt} is the number of individuals of species j with a tth location estimate, and I_j is the set of individuals of species j. Individuals with data gaps greater than 20 days were not included when calculating the number of individuals with location estimates for a given relative day of their track during the gap periods.

Under this weighting scheme, individual location estimates more proximal to the tagging location received a lower weight than later locations because more individuals had location estimates earlier in their tracks. Longer tracks received a higher total weight than shorter tracks because they had more location estimates. By increasing the weight of later locations and longer tracks, the calculated spatial density for these species should be more representative of natural spatial coverage and less affected by tag loss, failure, and a spatial bias toward deployment location.

Simulation tests indicated that our basic time weighting scheme was appropriate for very large sample sizes, but that it produced biased estimates of spatial density patterns when sample size was lower and more similar to the species-specific sample sizes in our study (*see next section*). To minimize this bias, we modified the basic time weighting scheme by implementing a threshold relative day of the track beyond which location weights were set equal to the weight on that threshold day. Simulation tests indicated that a threshold corresponding to the 85th percentile of track lengths for a given species approximately minimized the bias

across a range of scenarios with respect to sample size, movement, rate and distribution of tag loss and failure, and the resolution of the spatial density grid.

We applied a single threshold time weighting scheme to reduce the bias in spatial density patterns arising from tag loss and failure across many species. However, the overall multi-species density pattern was relatively robust to our choice of weighting scheme (Supplementary Fig. 10).

No weighting was applied to estimated locations of pinnipeds and seabirds where approximately 75-99% of tags were recovered and remained operational throughout the deployment duration; variance in track duration for these species is due largely to phenology (short vs. long migration of northern elephant seals), or individual variation in migration lengths, rather than tag loss or harvest. For these species, every location estimate was weighted equally ($w_{it} = 1$).

2.6.2 Simulation test of threshold time weighting scheme

We tested the appropriateness of our threshold time weighting scheme on simulated data where we knew the true underlying spatial density pattern.

Tracks were simulated according to a biased random walk movement model:

$$\mathbf{l}_t = \mathbf{l}_{t-1} + \mathbf{c} + \boldsymbol{\eta}_t \tag{14}$$

where $\mathbf{l}_t$ is a vector of length two describing the location of the animal at time t, $[x_t,\ y_t]$, $\mathbf{c}$ is a vector describing the bias in movement and $\boldsymbol{\eta}_t$ is the stochastic deviation in movement between times t and $t-1$, which is assumed to be normally distributed with mean 0 and variance-covariance matrix $\boldsymbol{\Sigma}$:

$$\boldsymbol{\Sigma} = \begin{pmatrix} \sigma_{\mathrm{x}}^2 & 0 \\ 0 & \sigma_{\mathrm{y}}^2 \end{pmatrix} \tag{15}$$

All simulated tracks were 100 time units long and originated at (0, 0) with a small amount of variability in the initial x location.

Three different movement scenarios were considered. In the first scenario, animals dispersed with a constant directional bias ($\mathbf{c} = [0, -0.1]$, $\sigma_{\mathrm{x}} = 1$, $\sigma_{\mathrm{y}} = 0.1$). In the second scenario, animals dispersed with a directional bias that reversed after half the time had elapsed ($\mathbf{c} = [-0.4, -0.4]$ for $t = 0$ to 50, $\mathbf{c} = [0.4, 0.4]$ for $t = 50$ to 100, $\sigma_{\mathrm{x}} = 0.5$, $\sigma_{\mathrm{y}} = 0.1$). In the third scenario, animals dispersed with no directional bias ($\mathbf{c} = [0, 0]$, $\sigma_{\mathrm{x}} = 0.5$, $\sigma_{\mathrm{y}} = 0.5$).

Tag loss and failure was simulated by drawing a sample of random track lengths from a probability distribution and truncating the simulated data tracks to those lengths. Three distributions were considered: exponential, gamma, and triangular. When a random track length exceeded the maximum track length, the maximum track length was used.

We then applied four different weighting schemes to the simulated track data with tag loss: 1) no weighting, 2) using only the longest 25% of tracks, 3) basic time weighting, and 4) threshold time weighting.

We compared spatial density maps for the full simulated tracks (the 'true' density) to density maps for the simulated data with tag loss and the four different weighting schemes. Density maps were derived by binning and summing the number of locations (or weights) on a spatial grid.

In addition to examining several movement scenarios and distributions of track lengths, we considered ranges of sample size, rate of tag loss and spatial grid resolution.

Correspondence between the true spatial density pattern and the spatial density pattern for data with tag loss and a given weighting scheme was assessed visually and by calculating the sum of squared differences in density between corresponding cells on the two grids. Density grids were first normalized to sum to 1 before calculating the sum of squares.

The results of this simulation analysis indicated that the basic time weighting scheme most closely matched the true spatial density pattern when sample size was very high (Supplementary Fig. 11). However, when sample size was smaller (e.g., 100 tracks), basic time weighting resulted in large biases whereby the ends of long tracks were overrepresented on the density map. Threshold time weighting performed better at small sample sizes because the weights at the ends of the longest tracks were smaller. Given the species-specific sample sizes in our actual data set, we decided to apply the threshold time weighting scheme to the real data.

Sample size also had a strong effect on the threshold percentile that resulted in the greatest correspondence (lowest sum of squares) between the true spatial density grid derived from simulated tracks and the corresponding density grid when tag loss and threshold time weighting were applied (Supplementary Fig. 12). As sample size increased, the optimal threshold increased. A threshold percentile of 100% corresponds to basic time weighting, so this result is consistent with the result that basic time weighting performed best when sample size was very large. For sample sizes of 50-100 tracks in our default scenario, the optimal threshold percentile was about 80-90%. Across the ranges of movement scenarios, rates of tag loss, distributions of track lengths and spatial grid resolutions explored, the optimal threshold percentile was generally between about 80% and 95%. In many cases the sum of squares tended to increase more rapidly as the threshold percentile increased beyond the optimal value, than it did as the threshold percentile decreased from the optimal value. Thus, it was better to underestimate the threshold percentile than to overestimate it, with respect to recovering the true spatial density pattern. Based on the results of this simulation analysis we chose to use a threshold percentile of 85% when applying the threshold time weighting scheme to the real data.

2.6.3 Normalization to account for unequal sample sizes among species

The total weights for each species were normalized to 1 so that within the study area each species contributed equally to the described multi-species density patterns:

$$d_{it} = w_{it} / \sum_{i \in I_j} \sum_{t=1}^{T_i} w_{it} \tag{16}$$

where d_{it} is the relative density contribution of the tth location estimate for individual i, and T_i is the number of location estimates for individual i. The relative density contributions for all location estimates for all individuals (d_{it}) were then summed within the longitudinal/latitudinal cells of the study area grid.

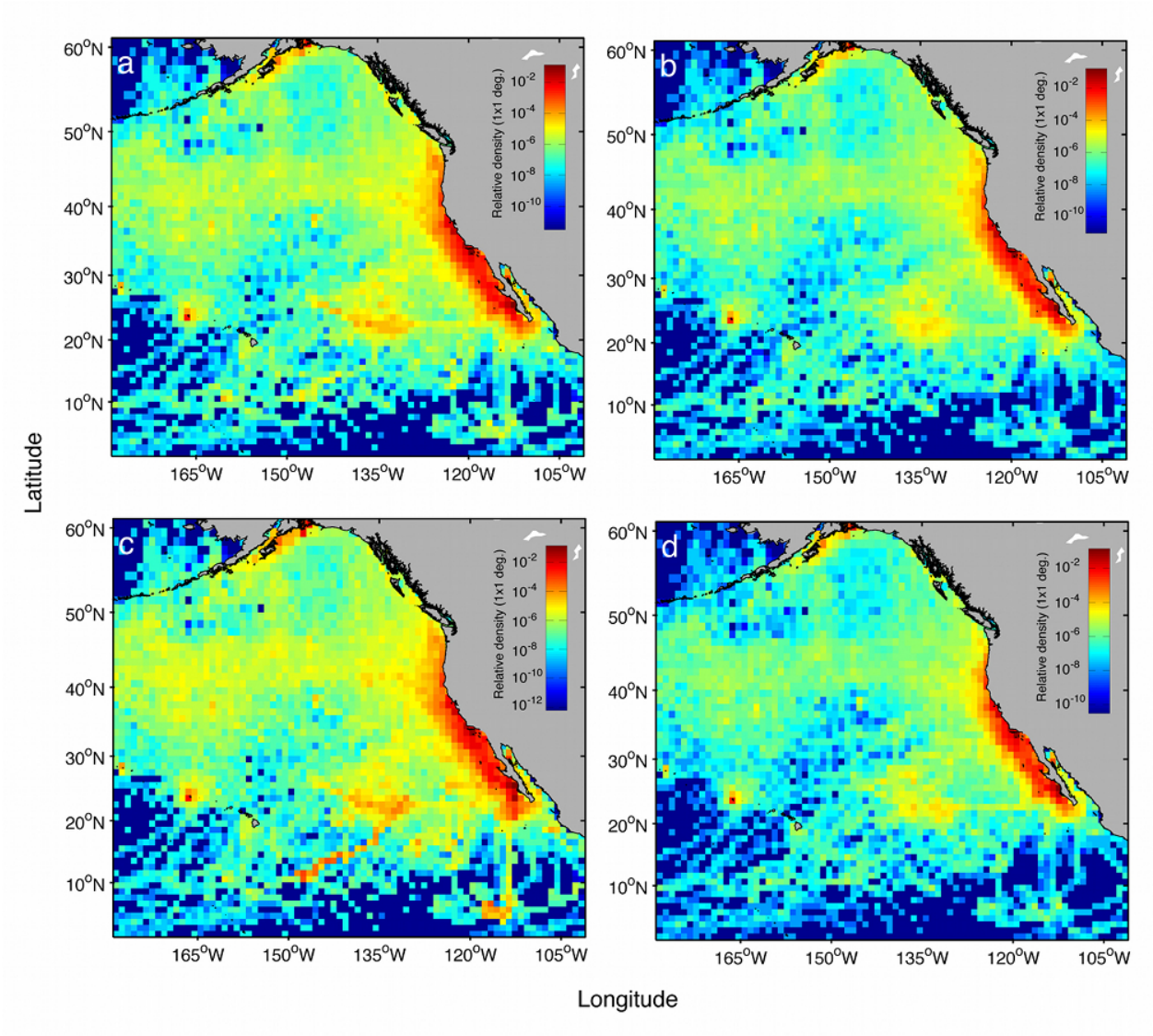

Supplementary Figure 10: Multi-species relative density in study area derived with four different weighting schemes: a) threshold time weighting (85%ile threshold), b) no time weighting, c) basic time weighting, and d) only using longest 25% of tracks for each species.

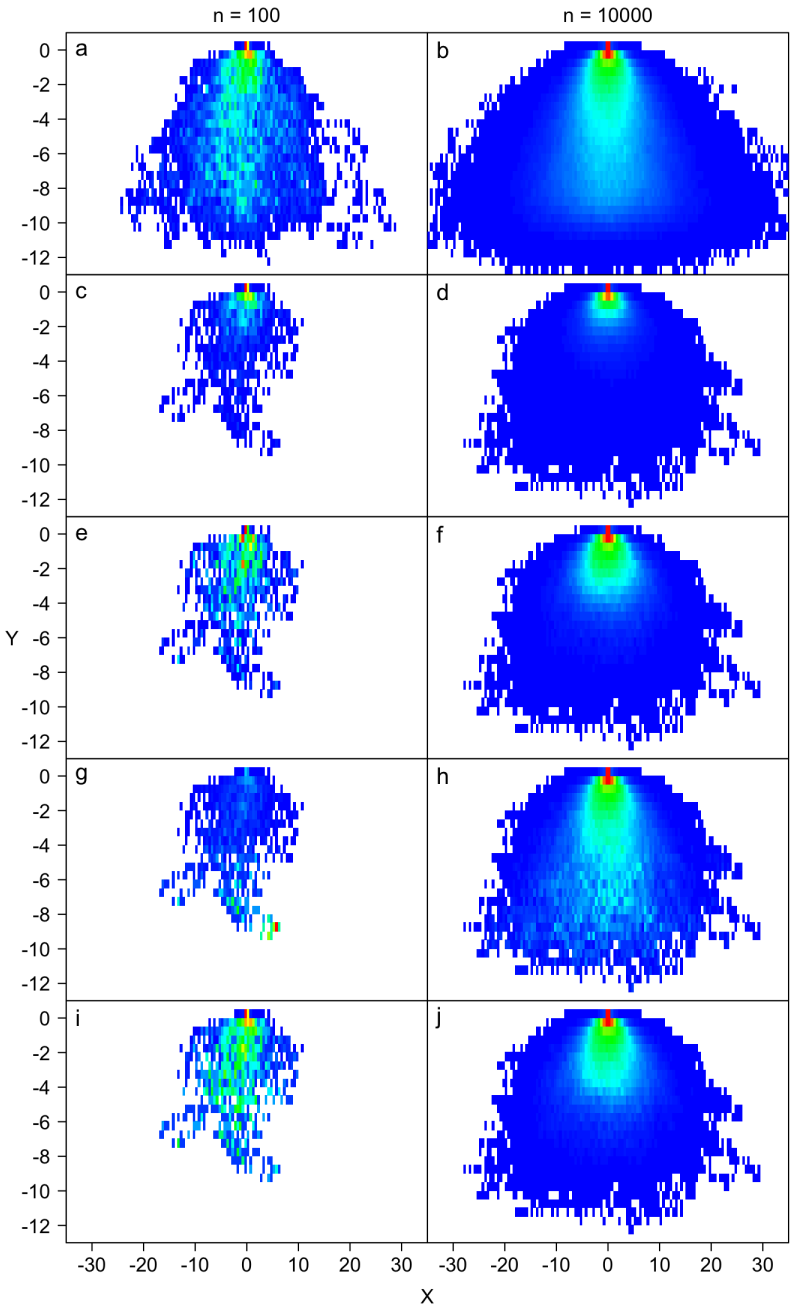

Supplementary Figure 11: Relative density grids for simulated tracks with two different sample sizes and four different weighting schemes. Red indicates highest density and blue indicates lowest density. Panels a and b represent the density derived from 100 and 10000 biased random walks, respectively (movement scenario 1). Spatial grid cells are 0.5 by 0.5. Panels c and d represent the density of these data after simulating tag loss and failure according to an exponential distribution of track lengths with a decay parameter of 0.05. Panels e and f represent the density of the longest 25% of tracks shown in panels c and d, respectively. Panels g and h represent the density of the data in panels c and d after basic time weighting was applied. Panels i and j represent the density of the data in panels c and d after threshold time weighting was applied with a threshold of the 85th percentile of track lengths.

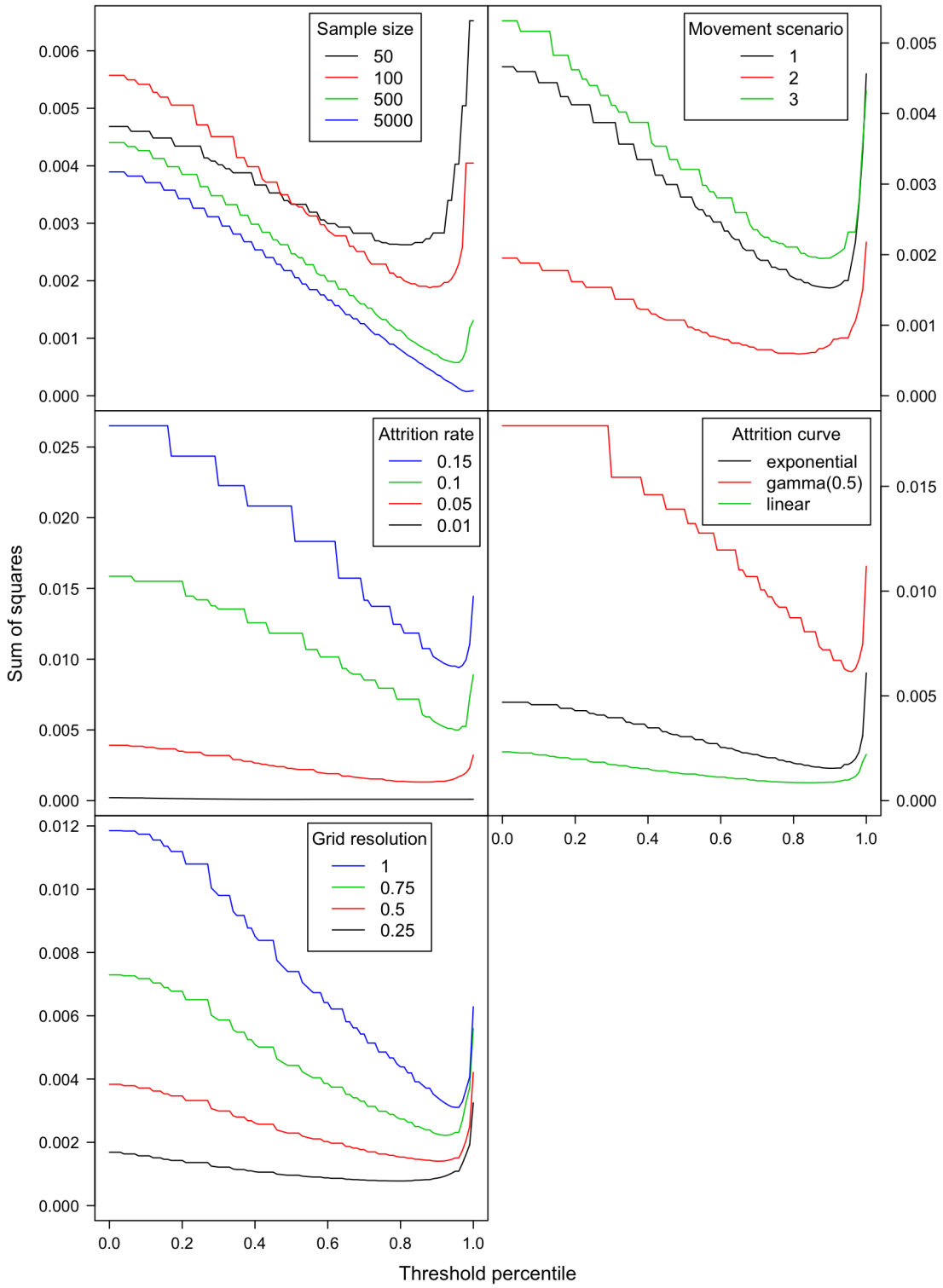

Supplementary Figure 12: Sum of squared differences between relative density grids for simulated tracks and relative density grids for the same tracks with simulated tag loss and threshold time weighting. Sum of squares is plotted by the threshold percentile. The five panels illustrate the effect of varying five parameters of interest (default values in parentheses): sample size (100 tracks), movement scenario (1), tag attrition decay rate (0.05), attrition curve or distribution of track lengths (exponential), and spatial grid resolution (0.5).

2.7 Null model simulations of animal movement

We employed a null model of animal movement to determine whether the observed density pattern could arise simply due to diffusion from the chosen tagging locations. We assumed that the observed movements can be approximated by a correlated random walk[59] with three fundamental parameters: mean turn angle, move persistence and move variability. These three parameters were estimated from the observed tracks with the state-space filtering model described in Eqns 1-5 as θ, γ and $\mathbf{\Sigma}$, respectively. These movement parameters effectively set the diffusion rate of a tagged "population". In other words, they determine the rate at which the tagged group of individuals spreads out from their initial tagging location.

To simulate animal movements, we first obtained averages of the three estimated parameters across all tagged individuals within each species. Then, using the process model described in Eqns 1-3, we simulated the same number of tracks as were observed and started the simulated tracks at the actual tagging locations for each species. We also ensured that the simulated tracks had the same distribution of durations as was observed for each species (see Table 1). We repeated this approach for a total of 5 replicates and, after applying the same threshold time-weighting and species normalizations as for the observed data (see Weighting and normalization), calculated the spatial density for all 5 replicates combined. This spatial density represents an approximation of the "simulated truth" with the 5 replicates serving to reduce Monte Carlo error. The simulated spatial densities were divided by 5 to facilitate comparison with the observed densities.

2.8 Relationships between predator distribution and oceanography

Time-weighted, species-normalized relative density data were modeled as a function of environmental variables to describe the functional relationship between top predator distribution and the environment of the northeastern Pacific Ocean study area.

2.8.1 Satellite data

We assembled time series of quarterly mean, median, standard deviation and median absolute deviation fields of satellite-derived oceanographic parameters (chlorophyll a (Chl), sea surface temperature (SST), sea surface height (SSH), and curl of wind stress). Bulk statistics were calculated for each available parameter within $1^\circ \times 1^\circ$ cells of the same grid used to calculate relative density (-180 to -100°E, 0 to 62°N) for a given quarter (21 June 2002 through 21 June 2009). Quarterly long-term medians (2002-2009) were also generated.

Chlorophyll a, derived from the Moderate Imaging Spectrometer using the OCM-3 algorithm[6], w0as chosen as a proxy for primary producers. The natural distribution of phytoplankton for the region of interest follows a log-normal distribution. Thus, we log-transformed the satellite-derived Chl for both display and analysis. Sea surface temperature fields were blended from a variety of infrared and microwave satellite sensors[61,62]. Sea surface height anomaly fields derived from the multiple satellite altimeters[63] were acquired from AVISO, Inc. Standard deviations of the SSH fields (SSHSD) were also calculated based on the SSH data present within each quarterly grid cell. The curl of the wind stress[64] was calculated from ocean surface vector winds[65] derived the SeaWinds instrument on the QuikSCAT spacecaft.

2.8.2 Generalized additive mixed models

Generalized additive mixed models (GAMMs) provided the best approach to modeling our data due to the non-linearity of many ecological relationships. We used a two-model approach to deal with the large number of zeroes, non-normality and non-constant variance of the relative density data. A binary habitat model was used to model presence/absence where 1° cell densities > 0 were coded as 1 and cell densities of zero were coded as 0. The presence/absence GAMM had a binomial likelihood and a logit link function. A relative habitat use model was used to model relative density within 1° cells with non-zero density. The relative habitat use GAMM had log-transformed relative density as the response, a Gaussian likelihood and an identity link function. The response was log-transformed to normalize the data and standardize their variance. Explanatory variables considered for both models were latitude, longitude, year, season (quarter), log(Chl) as a proxy for phytoplankton abundance, SST for thermal preferences, SSH and SSHSD as indicators of mesoscale activity, and wind stress curl as an estimate of oceanic convergence/divergence. Numerous works link increased biological activities to features that may be resolved by these properties[66,67]. Latitude and longitude were included as a measure of spatial structure resulting in no significant residual spatial autocorrelation in the residuals of either model. We assessed cross-correlation among the response and explanatory variables by examining pairwise Pearson's correlation coefficients. Year and quarter were treated as a random effect with each unique combination of year and quarter corresponding to a separate intercept. The GAMM models can be represented by the following equation:

$$\begin{aligned} y_{ijk} =& f_1(SST_{ijk}) + f_2(log(Chl_{ijk})) + f_3(latitude_{ijk}) + f_4(longitude_{ijk}) + \\ & f_5(SSH_{ijk}) + f_6(SSHSD_{ijk}) + f_7(windcurl_{ijk}) + \gamma_{jk} + \epsilon_{ijk} \end{aligned} \tag{17}$$

where y_{ijk} is logit(presence/absence) in the presence/absence model and log(relative density) in the relative density model for 1° grid cell i in quarter j of year k, f's represent spline functions of the explanatory variables, γ is a random intercept effect for each quarter-year combination and ϵ represents random error. Note that log(relative density) does not indicate a log link function but rather log-transformed response. Explanatory variable sets included in the final models were chosen based on the models with the lowest Akaike's Information Criterion (AIC). We assessed spatial autocorrelation in the relative density data and relative density model residuals using Moran's I statistic. All analyses were conducted using the statistical software R[68], and its libraries mgcv[69], nlme[70], spdep[71], ncf[72], and ape[73].

Cross-correlation coefficients were low except among latitude, SST and log chlorophyll-a. For the final relative density model we found that the global Morans I statistic was not significant at $\alpha = 0.05$ ($p = 0.062$) indicating that minimal spatial patterns remained in the residuals. For the presence/absence model the Moran's I statistic was also slightly non-significant ($p = 0.053$). Moran's I statistic values ranged from -0.0063 to 0.154 for the relative density model and -0.0003 to 0.046 for the presence/absence model across quarters and years.

We used the GAMM results to spatially map habitat with sea surface temperature and chlorophyll-a response values greater than zero. By overlaying normalized density values on these spatial grid cells, we created a Potential Habitat Utilization Index (PHUI) indicating where the highest relative use by the most TOPP species would be predicted as a function of temperature and chlorophyll (Supplementary Figure 3).

2.9 Niche separation within guilds

To test whether species within guilds experienced, on average, different SSTs, we fitted a linear mixed effects model[74] to the daily mean SST values for all tracks within a guild. We used the individual id as a grouping factor and an AR(1) autocorrelation structure for the within-individual errors and then tested for significant differences in average SST among species within a guild. The model had the following general form:

$$y_{(t)jk} = s_k + \gamma_{jk} + \epsilon_{(t)jk} \tag{18}$$

where $y_{(t)jk}$ is the mean SST on day t for individual j of species k, s_k is a factor representing the species, γ_{jk} is a random intercept for individual j of species k and $\epsilon_{(t)jk}$ is the within-individual error, such that:

$$\epsilon_{(t)jk} = \phi\epsilon_{(t-1)jk} + N(0, \sigma^2) \tag{19}$$

where ϕ is the lag 1 autocorrelation parameter.

We fitted this model separately to data from each of the following three guilds: albatrosses (Laysan and black-footed), tunas (Pacific bluefin and yellowfin), and lamnid sharks (shortfin mako, white and salmon). The white and salmon shark SST distributions were bimodal, indicative of the migration patterns of these species between areas characterized by distinctly different SST regimes. Accordingly, we estimate separate means for these different components of the white and salmon shark SST distributions by introducing two additional levels to the species factor, s_k, one for each species. All models were fit using Maximum Likelihood estimation in R[68] with the nlme package[70].

3 Supplementary Discussion

3.1 Null model simulations of animal movement

The simulated spatial densities indicate the pattern arising from species-specific diffusion away from initial tagging locations. The dominant hotspot is centred on the CCLME, with density declining farther to the north, south and west (Supplementary Fig. 5). Smaller hotspots are evident in Prince William Sound, where salmon sharks were tagged (top of Supplementary Fig. 5), and French Frigate Shoals, where Laysan and Black-footed albatrosses were tagged (northwestern Hawaiian Islands).

Despite the high concentration of tagging effort within the CCLME, observed densities of tagged predators within the CCLME are generally higher than expected based on the simulations (Supplementary Fig. 5). Although observed densities are similar to the simulated densities within the California Bight portion of CCLME, they tend to be higher immediately adjacent to the coast north of the Bight and higher throughout much of the southern CCLME (adjacent to the Baja Peninsula; Supplementary Fig. 5). Observed densities decline sharply at the 200 nmi limit of the Can-US-Mexico EEZ's, whereas simulated densities decline much more gradually with distance from the US coast (compare Supplementary Fig. 5 a and b). Finally,

the simulations greatly under-predict the density of predators within the north Pacific Transition Zone and along the Alaskan coast, west of Prince William Sound (Supplementary Fig. 5c).

Combined, these results suggest that the observed spatial density of tagged predators in the north Pacific is not due simply to the tagging design employed and subsequent diffusion of tagged animals.

3.2 Fidelity to the CCLME

In the main text, we illustrate with a selection of tracks of different species the fidelity of large predators to the CCLME (Fig. 2). Here we support these statements with a comparison of the observed and expected mean proportion of time spent by each species within the CCLME. We refer to fidelity as either the attraction of predators, tagged at distant locations, to the CCLME or the retention of predators tagged within the CCLME. We use the null model simulation, described above, to generate the expectation for each species and calculate binomial 95% confidence intervals for the observed mean proportion of time spent within the CCLME. The test is two-sided as species can spend either more or less time within the CCLME than expected based on the null movement model.

We grouped species according to whether they were tagged in the CCLME or outside; species tagged outside the CCLME generally had both lower expected and observed mean proportion of time spent in the CCLME than species tagged within the CCLME (Supplementary Fig. 6). Eleven of 17 tests revealed a significant difference between expected and observed mean proportion of time spent in the CCLME. Species tagged in the CCLME showed variable patterns against their expected mean proportion of time in the CCLME (Supplementary Fig. 6a). In general, species tagged outside of the CCLME spent significantly more time in the CCLME than expected, including very long distance migrants; leatherback turtles tagged in Indonesia and sooty shearwaters tagged in New Zealand (Supplementary Fig. 6b). With the exception of short-finned mako sharks, California sea lions and blue whales, the non-significant differences occurred for species with low sample sizes. For species that spent a significantly lower proportion of time in the CCLME than expected, two are return migrants (white shark and northern elephant seals), and the Monterey-tagged leatherback turtles were likely making return migrations to nesting beaches in the western.

3.3 Relationships between predator distribution and oceanography

3.3.1 Satellite data

Many TOPP species made N-S migrations in concert with seasonal changes in oceanic condition as shown by monthly Chl and SST climatologies (Fig. 3b, Supplementary Fig. 3). As temperature increased and productivity decreased in the southern region of the California Current System (CCS), the median latitude for tunas, sharks, and blue whales also moved northward. Seabirds and pinnipeds did not show the same north-south migration in concert with temperature. Instead they were generally found further north, demonstrating a different use of the thermal and foraging seascape in the CCS than other guilds.

3.3.2 Generalized additive mixed models

The fitted relative density model with the lowest AIC included all explanatory variables; the presence/absence model with the lowest AIC excluded latitude and sea surface height standard deviation (Supplementary Tables 7 and 8).

Supplementary Table 7: Summary statistics of fitted GAMMs. Morans I statistic was calculated from the residuals of the fitted models and can range from -1 to 1 with values > 0 indicating spatial clustering and values < 0 indicating dispersion. Morans I statistic p-values indicate that there was residual but non-significant spatial clustering in the presence/absence model and in the relative density model.

	Presence/absence	Relative density
Proportion of deviance explained	0.303	0.232
AIC	598375	74780.45
Moran's I statistic	0.013	0.050
Moran's I p-value	0.053	0.062

Supplementary Table 8: Model variables in final fitted presence/absence and relative density GAMMs.

Explanatory variable	Estimated DF	F	p-value
Presence/absence			
s(Xsst)	3.986	2506.99	< 0.001
s(log(Xchl))	3.945	1077.67	< 0.001
s(Xlon)	3.979	131.35	< 0.001
s(Xssh)	3.867	20.3	< 0.001
s(Xcurl2b)	3.935	58.6	< 0.001
Relative density			
s(Xsst)	3.90	31.01	< 0.001
s(log(Xchl))	3.95	226.84	< 0.001
s(Xlat)	3.94	122.57	< 0.001
s(Xlon)	3.97	147.62	< 0.001
s(Xssh)	1.48	72.25	< 0.001
s(Xsshstd)	3.31	20.11	< 0.001
s(Xcurl2b)	3.78	26.63	< 0.001

By using both presence/absence and relative density models we were able to differentiate cells that top predators used at least once from cells that were frequently used by the normalized species and individual density. The results from the presence/absence model show that the majority of habitat used by top predators was found at waters near 15°C but across many chlorophyll-a concentrations. When looking at use within identified habitat, relative density was greatest in cells with high chlorophyll-a concentrations.

The estimated relationship between the probability of presence and SST was convex with a peak at about 15°C (Supplementary Fig. 13a). Presence had a more complicated relationship with log(chlorophyll-a) peaking at values of -1 (0.1 mg/m^3 Chl-a). Presence relative to longitude increased from 180 to 120°W peaking at the CCS. Probability of presence was greatest around SSH values of 0. There was no significant pattern between presence/absence and curl at extreme values but there was a strong positive relationship

with positive curl values between 0 and 1×10^{-6}.

There was a positive relationship between relative density and SST that peaked between 20-25°C (Supplementary Fig. 13b). The relationship between relative density and chlorophyll-a was also positive. The relationships between relative density, latitude and longitude indicate the importance of the CCS and Southern California Bight while the longitude relationship shows a small second peak near Hawaii. Relative density had a positive relationship with sea surface height but a negative relationship with the standard deviation of SSH. There was a concave relationship between relative density and wind curl with the estimated minimum around -2.5$\times10^{-7}$.

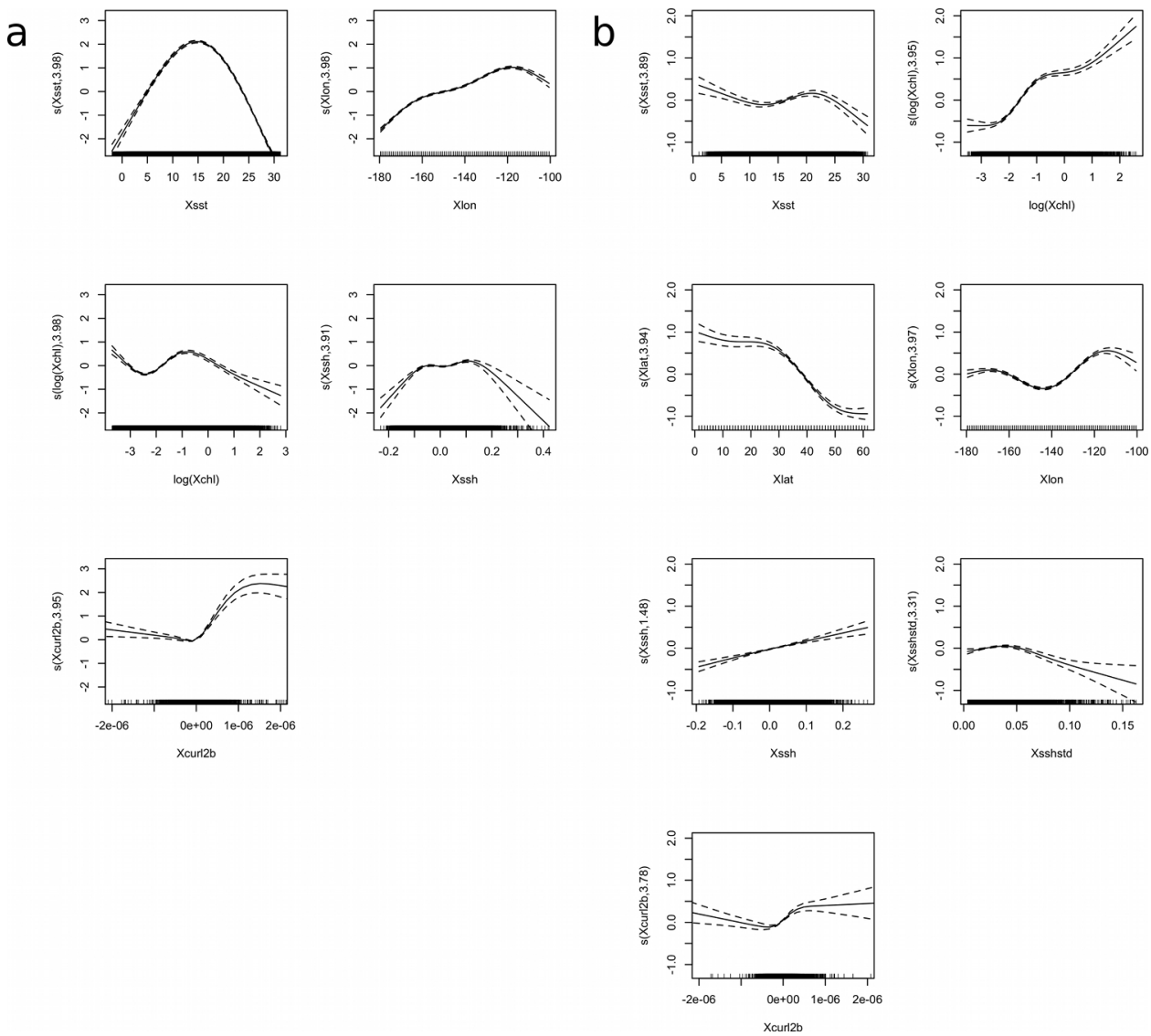

Supplementary Figure 13: Estimated relationships between presence/absence (a) and relative density (b) and explanatory variables in final fitted GAMMs.

3.4 Niche separation within guilds

3.4.1 Albatrosses

The linear mixed-effects (LME) model revealed a significant difference between mean SSTs experienced by Laysan and black-footed albatrosses (Supplementary Table 9). The standard deviation of the random effect (individual) was small, implying little among individual variation in mean SSTs experienced. Autocorrelation (lag 1) of daily SSTs within individuals was high (ϕ = 0.97) and comparison of AICs and the likelihood ratio for models with and without an AR(1) correlation structure strongly favoured the AR(1) formulation (Δ AIC = 13,664; L ratio = 13,666, p $\leq$ 0.0001).

Supplementary Table 9: Summary of linear mixed-effects model fit to daily SSTs for black-footed and Laysan albatrosses. The intercept term is the mean SST for black-footed and s_2 represents the difference in mean SST between Laysan and black-footed albatrosses. The standard deviation of the random effects term was 0.0018, with a residual error of 5.20.

Term	Value	S.E.	df	t-value	p-value
Intercept	17.84	0.55	8,667	32.60	0
s_2	-3.87	0.73	53	-5.30	0

3.4.2 Tunas

The linear mixed-effects (LME) model revealed a significant difference between mean SSTs experienced by Pacific bluefin and yellowfin tunas (Supplementary Table 10). The standard deviation of the random effect (individual) was moderate, implying some among-individual variation in mean SSTs experienced. Autocorrelation (lag 1) of daily SSTs within individuals was high (ϕ = 0.96) and comparison of AICs and the likelihood ratio for models with and without an AR(1) correlation structure strongly favoured the AR(1) formulation (Δ AIC = 171,833.3; L ratio = 171,835.3, p $\leq$ 0.0001).

Supplementary Table 10: Summary of linear mixed-effects model fit to daily SSTs for Pacific bluefin and yellowfin tunas. The intercept term is the mean SST for bluefin and s_2 represents the difference in mean SST between yellowfin and bluefin tunas. The standard deviation of the random effects term was 0.91, with a residual error of 2.02.

Term	Value	S.E.	df	t-value	p-value
Intercept	17.36	0.09	74,801	190.54	0
s_2	4.19	0.14	374	29.50	0

3.4.3 Sharks

The linear mixed-effects (LME) model revealed a significant difference between mean SSTs experienced by shortfin mako and salmon sharks and between shortfin mako and white sharks (α = 0.05; Supplementary Table 11). White and salmon sharks occupied similar SST space in the 10 - 15 °C range, as judged by overlap in their respective 95% confidence intervals, but otherwise used distinctly warmer and colder waters, respectively (Fig. 5). The standard deviation of the random effect (individual) was small, implying little among-individual variation in mean SSTs experienced. Autocorrelation (lag 1) of daily SSTs within individuals was high (ϕ = 0.97) and comparison of AICs and the likelihood ratio for models with and without an AR(1) correlation structure strongly favoured the AR(1) formulation (Δ AIC = 27,350.13; L ratio = 27,352.14, p $\leq$ 0.0001).

Supplementary Table 11: Summary of linear mixed-effects model fit to daily SSTs for shortfin mako, salmon and white sharks. The intercept term is the mean SST for shortfin mako, ss_c represents the difference in mean SST between salmon sharks in colder waters and shortfin mako sharks, ss_w represents the difference in mean SST between salmon sharks in warmer waters and shortfin mako sharks, and similarly for white sharks (ws_c and ws_w). The standard deviation of the random effects term was 0.02, with a residual error of 3.07.

Term	Value	S.E.	df	t-value	p-value
Intercept	18.49	0.30	12,830	62.53	0
ss_c	-11.57	0.38	134	-30.77	0
ss_w	-5.06	0.37	134	-13.51	0
ws_c	-6.14	0.37	134	-16.56	0
ws_w	2.59	0.37	134	6.98	0

Supplementary Notes

31 Le Boeuf, B. J., Crocker, D. E., Costa, D. P., Blackwell, S. B., Webb, P. M., and Houser, D. S. Foraging ecology of northern elephant seals. *Ecological Monographs* **70**, 353–382 (2000).

32 James, M. C., Myers, R. A., and Ottensmeyer, C. A. Behaviour of leatherback sea turtles, *Dermochelys coriacea*, during the migratory cycle. *Proceedings of the Royal Society of London, Series B* **272**, 1547–1555 (2005).

33 Shaffer, S. A., Tremblay, Y., Awkerman, J. A., Henry, R. W., Teo, S. L. H., Anderson, D. J., Croll, D. A., Block, B. A., and Costa, D. P. Comparison of light- and SST-based geolocation with satellite telemetry in free-ranging albatrosses. *Marine Biology* **147**, 833–843 (2005).

34 Teo, S., Boustany, A., Dewar, H., Stokesbury, M., Weng, K., Beemer, S., Seitz, A., Farwell, C., Prince, E., and Block, B. Annual migrations, diving behavior, and thermal biology of Atlantic bluefin tuna, *Thunnus thynnus*, on their Gulf of Mexico breeding grounds. *Marine Biology* **151**(1), 1–18 (2007).

35 Weng, K., Foley, D., Ganong, J., Perle, C., Shillinger, G., and Block, B. Migration of an upper trophic level predator, the salmon shark *Lamna ditropis*, between distant ecoregions. *Marine Ecology Progress Series* **372**, 253–264 (2008).

36 Mate, B., Mesecar, R., and Lagerquist, B. The evolution of satellite-monitored radio tags for large whales: One laboratory's experience. *Deep Sea Research Part II: Topical Studies in Oceanography* **54**(3-4), 224–247 (2007).

37 Wilson, R. P., Ducamp, J. J., Rees, W. G., Culik, B. M., and Nickamp, K. Estimation of location: global coverage using light intensity. In Wildlife telemetry: remote monitoring and tracking of animals, Priede, I. G. and Swift, S. M., editors, 131–134. Ellis Horwood, New York (1992).

38 Hill, R. D. Theory of geolocation by light levels. In Elephant seals: population ecology, behavior, and physiology, Le Boeuf, B. J. and Laws, R. M., editors, 227–236. University of California Press, Berkeley, California, USA (1994). 414 pp.

39 Teo, S. L. H., Boustany, A., Blackwell, S., Walli, A., Weng, K. C., and Block, B. A. Validation of geolocation based on light level and sea surface temperature from electronic tags. *Marine Ecology Progress Series* **283**, 81–98 (2004).

40 Block, B., Dewar, H., Farwell, C., and Prince, E. A new satellite technology for tracking the movements of Atlantic bluefin tuna. *Proceedings of the National Academy of Sciences of the United States of America* **95**(16), 9384 (1998).

41 Block, B., Dewar, H., Williams, T., Prince, E., Farwell, C., and Fudge, D. Archival tagging of Atlantic bluefin tuna (Thunnus thynnus thynnus). *Marine Technology Society Journal* **32**(1), 37–46 (1998).

42 Boustany, A. M., Davis, S. F., Pyle, P., Anderson, S. D., Le Boeuf, B. J., and Block, B. A. Expanded niche for white sharks. *Nature* **415**, 35–36 (2002).

43 Weise, M. and Costa, D. Total body oxygen stores and physiological diving capacity of California sea lions as a function of sex and age. *Journal of Experimental Biology* **210**(2), 278 (2007).

44 Bailey, H., Shillinger, G., Palacios, D., Bograd, S., Spotila, J., Paladino, F., and Block, B. Identifying and comparing phases of movement by leatherback turtles using state-space models. *Journal of Experimental Marine Biology and Ecology* **356**, 128–135 (2008).

45 Vincent, C., McConnell, B. J., Fedak, M. A., and Ridoux, V. Assessment of ARGOS location accuracy from satellite tags deployed on captive grey seals. *Marine Mammal Science* **18**, 301–322 (2002).

46 Lunn, D. J., Thomas, A., Best, N., and Spiegelhalter, D. WinBUGS - a Bayesian modelling framework: concepts, structure, and extensibility. *Statistics and Computing* **10**, 325–337 (2000).

47 Brooks, S. P. and Gelman, A. General methods for monitoring convergence of iterative simulations. *Journal of Computational and Graphical Statistics* **7**(4), 434–455 (1998).

48 Sibert, J. R., Musyl, M. K., and Brill, R. W. Horizontal movements of bigeye tuna near Hawaii from archival tagging data. *Fisheries Oceanography* **12**, 141–151 (2003).

49 Nielsen, A., Bigelow, K. A., Musyl, M. K., and Sibert, J. R. Improving light-based geolocation by including sea surface temperature. *Fisheries Oceanography* **15**, 314–325 (2006).

50 Normand, S.-L. T. Meta-analysis: formulating, evaluating, combining and reporting. *Statistics in Medicine* **18**, 321–359 (1999).

51 Morales, J. M., Haydon, D. T., Friar, J., Holsinger, K. E., and Fryxell, J. M. Extracting more out of relocation data: building movement models as mixtures of random walks. *Ecology* **85**, 2436–2445 (2004).

52 Jonsen, I. D., Myers, R. A., and James, M. C. Identifying leatherback turtle foraging behaviour from satellite telemetry using a switching state-space model. *Marine Ecology Progress Series* **337**, 255–264 (2007).

53 Patterson, T. A., Basson, M., Bravington, M. V., and Gunn, J. S. Classifying movement behaviour in relation to environmental conditions using hidden Markov models. *Journal of Animal Ecology* **78**, 1113–1123 (2009).

54 Martínez-Beneito, M. A., Conesa, D., López-Quílez, A., and López-Maside, A. Bayesian Markov switching models for the early detection of influenza epidemics. *Statistics in Medicine* **27**, 4455–4468 (2008).

55 Hamilton, J. D. A new approach to the economic analysis of nonstationary time series and the business cycle. *Econometrica* **57**(2), 357–384 (1989).

56 Kim, C.-J. and Nelson, C. R. *State-space models with regime switching: Classical and Gibbs-sampling approaches with applications*. The MIT Press, Cambridge, USA, (1999).

57 Mangel, M. and Clark, C. W. *Dynamic modeling in behavioral ecology*. Monographs in behavior and ecology. Princeton University Press, Princeton, New Jersey, (1988).

58 Breed, G. A., Jonsen, I. D., Myers, R. A., Bowen, W. D., and Leonard, M. L. Sex-specific, seasonal foraging tactics of adult grey seals (*Halichoerus grypus*) revealed by state-space analysis. *Ecology* **90**, 3209–3221 (2009).

59 Turchin, P. *Quantitative Analysis of Movement: Measuring and modeling population redistribution in animals and plants*. Sinauer Associates, Sunderland, (1998).

60 O'Reilly, J. E. and 21 co-authors. Ocean color chlorophyll a algorithms for SeaWiFS, OC2, and OC4: Version 4. In O'Reilly, J E and 24 co-authors, 2000: SeaWiFS postlaunch calibration and validation analyses, part 3. NASA Tech. Memo. 2000-206892, Hooker, S. B. and Firestone, E. R., editors, volume 11, 9–23. NASA Goddard Space Flight Center, Greenbelt, Maryland, USA (2000).

61 Powell, B. S., Arango, H., Moore, A., Di Lorenzo, E., Milliff, R., and Foley, D. 4DVAR data assimilation in the Intra-Americas Sea with the Regional Ocean Modeling System (ROMS). *Ocean Modelling* **23**, 130–145 (2008).

62 Veneziani, M., Edwards, C. A., Doyle, J. D., and Foley, D. A central California coastal ocean modelling study: 1. Forward model and the influence of realistic versus climatological forcing. *Journal of Geophysical Research* **114**(C04015) (2009).

63 Ducet, N., Le Traon, P.-Y., and Reverdin, G. Global high resolution mapping of ocean circulation from Topex/Poseidon and ERS-1 and -2. *Journal of Geophysical Research* **105**(C8), 19477–19498 (2000).

64 Gill, A. E. Atmosphere-ocean dynamics. In *International geophysics series*, volume 30, 326–328. Academic, San Diego, CA (1982).

65 Smith, S. D. Coefficients for sea surface wind stress, heat flux, and wind profiles as a function of wind speed and temperature. *Journal of Geophysical Research* **93**(C12), 15467–15472 (1988).

66 Bograd, S. J., Foley, D. G., Schwing, F. B., Wilson, C., Laurs, R. M., Polovina, J. J., Howell, E. A., and Brainard, R. E. On the seasonal and interannual migrations of the transition zone chlorophyll front. *Geophysical Research Letters* **31**(17), L17204 (2004).

67 Palacios, D. P., Bograd, S. J., Foley, D. G., and Schwing, F. B. Oceanographic characteristics of biological hot spots in the North Pacific: a remote sensing perspective. *Deep-Sea Research II* **53**(3-4), 250–269 (2006).

68 R Development Core Team. *R: A language and environment for statistical computing, version 2.8.1*. Foundation for Statistical Computing, Vienna, Austria, (2009).

69 Wood, S. N. Fast stable direct fitting and smoothness selection for generalized additive models. *Journal of the Royal Statistical Society B* **70**(3), 495–518 (2008).

70 Pinheiro, J. C., Bates, D., DebRoy, S., and Sarkar, D. nlme: linear and nonlinear mixed effects models. R package version 3.1-96, (2008).

71 Bivand, R., Anselin, L., Berke, O., Bernat, A., Carvalho, M., Chun, Y., Dormann, C., Dray, S., Halbersma, R., Lewin-Koh, N., Ono, H., Peres-Neto, P., Tiefelsdorf, M., and Yu, D. spdep: Spatial dependence: Weighting schemes, statistics and models. R package version 0.4-59, (2005).

72 Bjørnstad, O. N. ncf: spatial nonparametric covariance functions. R package version 1.1-3, (2006).

73 Paradis, E. *Analyses of phylogenetics and evolution with R*. Springer, New York, USA, (2006).

74 Pinheiro, J. C. and Bates, D. M. *Mixed-Effects Models in S and S-PLUS*. Springer-Verlag, New York, (2000).